ACS OMEGA

Open Access

http://pubs.acs.org/journal/acsodf

Article

Benzyloxychalcone Hybrids as Prospective Acetylcholinesterase Inhibitors against Alzheimer's Disease: Rational Design, Synthesis, In Silico ADMET Prediction, QSAR, Molecular Docking, DFT, and Molecular Dynamic Simulation Studies

Helmi Mohammed Al-Maqtari, Aso Hameed Hasan, Mustapha Suleiman, Muhammad Asraf Ahmad Zahidi, Mahmoud A. Noamaan, Pavel Alexyuk, Madina Alexyuk, Andrey Bogoyavlenskiy, and Joazaizulfazli Jamalis*

Cite This: *ACS Omega* 2024, 9, 32901−32919

Read Online

ACCESS | Metrics & More | Article Recommendations | Supporting Information

ABSTRACT: Acetylcholinesterase inhibitors (AChEIs) are crucial therapeutic targets for both the early and severe stages of Alzheimer's disease (AD). Chalcones and their chromone-based derivatives are well-known building blocks with anti-Alzheimer properties. This study synthesized 4-benzyloxychalcone derivatives and characterized their structures using IR, ^{1}H NMR, ^{13}C NMR, and HRMS. Additionally, the synthesized 4-benzyloxychalcone derivatives were tested for anti-acetylcholinesterase (AChE) activity. The synthesized compounds outperformed galantamine, which is used as a positive control against acetylcholinesterase. Utilizing an acetylcholinesterase (AChE) receptor (PDB ID: 4EY7)-chalcone derivative (**12a-c**), a molecular docking investigation was performed on the synthesized compounds. The goal was to predict the binding sites and energies of the derivatives with respect to the receptor amino acids. The dynamic behavior of the ligand−receptor complex resulting from the interaction of the best docking compounds **12a** and **12c** with the acetylcholinesterase receptor was used to analyze the stability *via* MD simulation. MM/GBSA and MM/PBSA were used to calculate free binding energies using snapshots from system trajectories. Advanced computational approaches incorporating long-range corrections were utilized to calculate the molecular characteristics of chalcone derivatives **12a-c** at the DFT/wB97XD/6-311++G(d,p) level. We used the molecular electrostatic surface potential (MESP) with high-quality data and visualization to find the most active site in these molecules. Reactivity descriptors, including the condensed Fukui function, chemical hardness (η), dual descriptors, chemical potential (μ), and electrophilicity (ω), were calculated for the chalcone derivatives.

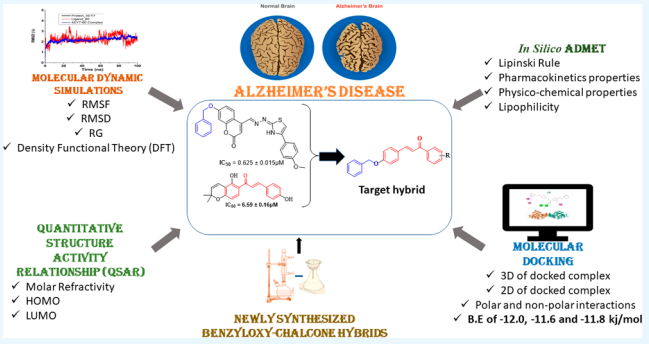

1. INTRODUCTION

Chalcones, also known as benzylideneacetophenones, are recognized as important compounds found in natural resources. These molecules, known as 1,3-diaryl-2-propen-1-ones, are part of the plant flavonoid family and are commonly known as open-chain flavonoid molecules.[1] Chalcone is an aromatic molecule consisting of two aromatic rings connected by a three-carbon α,β-unsaturated carbonyl system.[1,2] Chalcones are widely found in nature and range from ferns to higher plants, as reported in previous research.[3] The biosynthesis of isoflavonoids and flavonoids also involves the utilization of chalcones as open-chain precursors. This process mostly results in the formation of polyphenolic compounds that exhibit a color transition from yellow to orange. The chalcones can exist in two forms: *trans* (*E*) **1** or *cis* (*Z*) **2** isomers (Figure 1). The *trans* isomer is more thermodynamically stable than the *cis* isomer, making it the most common

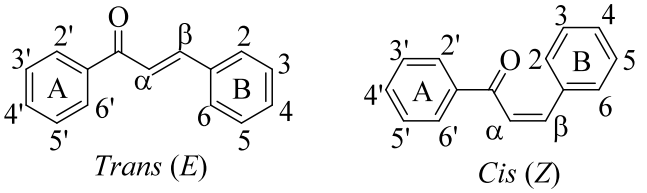

Figure 1. Structures of *trans* (**1**) and *cis* (**2**) chalcones.

Received: April 16, 2024
Revised: June 27, 2024
Accepted: June 28, 2024
Published: July 20, 2024

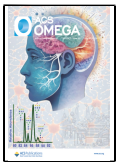

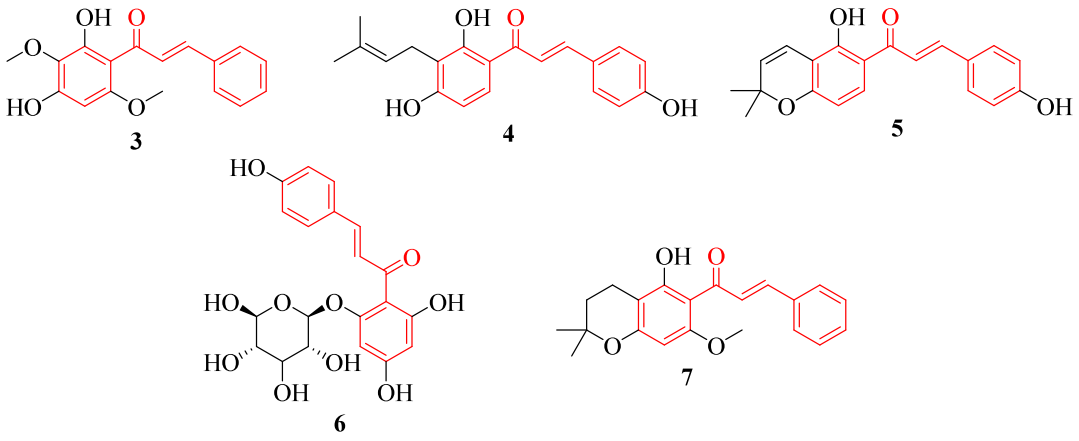

Figure 2. Chalcones as inhibitors of acetylcholinesterase.

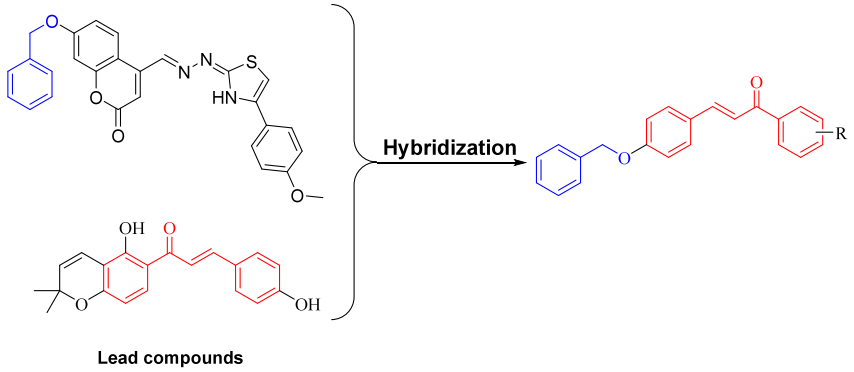

Figure 3. Representation of the lead compounds and the designed target hybrids.

chalcone configuration.[4] The *Z* isomer's configuration is considered unstable due to the significant steric effects resulting from the interaction between the A-ring and the carbonyl functional group.[5]

Chalcones exhibit a conjugated double bond that leads to the delocalization of π-electrons across both aromatic rings toward the carbonyl carbon, hence decreasing their electrophilicity. The chalcone nucleus has been identified as the primary intermediate and is a crucial component of several flavonoids and therapeutic compounds. The primary method for synthesizing chalcone involves the Claisen−Schmidt reaction, which occurs when aromatic aldehydes react with aromatic ketones in the presence of acid or base catalysts.[6] Chalcone serves as a crucial intermediary or starting material for producing different derivatives, including thiazine, pyrazoline, cyanopyridine, oxazoline and isoxazole. This is achieved through the cyclization of the α,β-unsaturated carbonyl group in chalcone. The resulting derivatives can have various heterocyclic ring systems attached to one or both of the aromatic rings.[7−9] Therefore, chalcone is highly important in the field of medicinal medication design.[5] Chalcones have been extensively explored and found to have numerous advantageous biological properties, such as anti-inflammatory, antibacterial, antifungal, anticancer, antioxidant and antitoxicity.[2,10,11] Chalcones provide protection against viruses, UV radiation and parasites in plants. Additionally, their antioxidant and anti-inflammatory qualities make them highly relevant in the treatment of human illnesses such as malaria, cancer, tuberculosis and asthma.[12]

Alzheimer's disease (AD) is a chronic neurodegenerative disorder linked to the aging process. It causes a gradual and irreversible decline in cognitive function, including memory loss, deterioration of language skills, dementia and cognitive impairment.[13] Researchers have presented the cholinergic hypothesis as a crucial theoretical framework for treating Alzheimer's disease (AD). In the brain, this illness causes tissue loss and the death of nerve cells. Almost all of the brain's activities are affected by the drastic shrinkage that occurs over time.[14] Preserving cholinergic functioning has the potential to reduce these symptoms.[15,16] Several medications have received approval for the therapeutic management of AD, but nevertheless, they do not significantly influence the progression of the disease.[17,18] Multiple studies have demonstrated the capacity of chalcone, which is derived from plant natural products, to function as an inhibitor of acetylcholinesterase (AChE) in neurodegenerative conditions. Therefore, flavonoids that can inhibit acetylcholinesterase (AChE) are the most favorable candidates for Alzheimer's disease (AD) treatment.[2] Figure 2 shows the chalcone compounds that have a natural origin and excellent anti-Alzheimer's disease activity, specifically 2′,4′-dihydroxy-3′,6′-dimethoxychalcone **3** from Polygonum *limbatum* leaves and isobavachalcone **4** and 4-hydroxylonchocarpin **5** from *Dorstenia barteri* twig leaves. These compounds were isolated and assessed for their ability to inhibit acetylcholinesterase (AChE) activity.[19] The researchers reported that compound **3** (IC_{50} = 6.05 ± 0.11 μg/mL) and compound **5** (IC_{50} = 6.59 ± 0.16 μg/mL) exhibited inhibitory activity, while compound **4** (IC_{50} = 5.93 ± 0.13 μg/mL) demonstrated significant activity against

https://doi.org/10.1021/acsomega.4c03679
ACS Omega 2024, 9, 32901−32919

Scheme 1. Synthesis of 4-Benzyloxychalcones 12a-c[a]

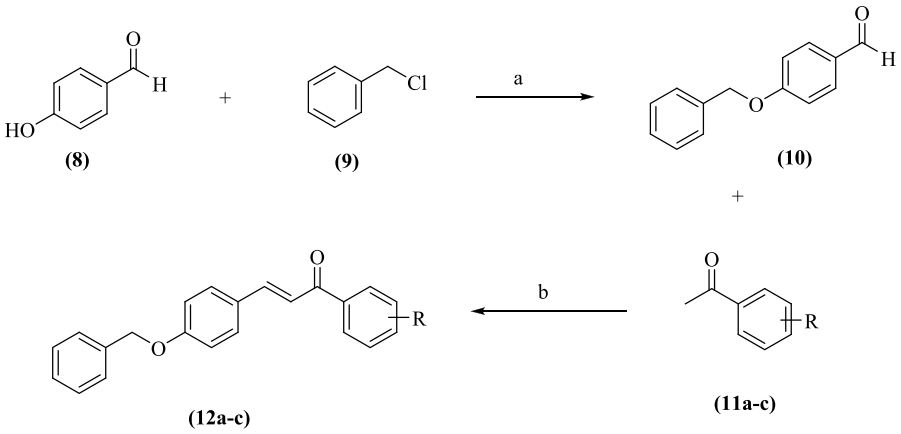

Compound	R
12a	4-benzyloxy
12b	4-I
12c	CH_3

[a]Reagents and conditions: (a) ethanol, K_2CO_3, reflux 6 hr; (b) NaOH, ethanol, 8 hr.

acetylcholinesterase, which is comparable to that of the standard drug Eser (IC_{50} = 4.94 ± 0.05 μg/mL). The compound isosalipurposide **6** also exhibited prominent activity on AChE, and it was derived from the flowers of *Acacia cyanophylla*.[20] Chemical **6** has been shown to be efficacious against acetylcholinesterase, with an IC_{50} value of 52.04 μg/mL. In addition, Sribuhom et al. (2016) extracted obovatachalcone **7** from the seed of *Derris indica*, which exhibited greater efficacy against AChE than did tacrine;[21] therefore, developing new selective compounds for anti-AD medication development is a major breakthrough in AD treatment. Given the aforementioned limitations in terms of the drugs available, the objective of this research work was to modify chalcone moieties to enhance their ability to provide excellent inhibition of acetylcholinesterase, the lead compounds and the designed target hybrids are shown in Figure 3. In addition, the bioassays were performed using molecular docking, molecular dynamics (MD) modeling, quantitative structure−activity relationship (QSAR), and chemical reactivity methods.

2. RESULTS AND DISCUSSION

2.1. Synthesis and Characterization of the Title Compounds (12a-c). Compounds (**12a-c**) were synthesized as depicted in Scheme 1. Briefly, the starting material of 4-benzyloxybenzaldehyde **10** was synthesized *via* Williamson ether synthesis to obtain chalcone derivatives.[2] This reaction method was employed using equimolar amounts of appropriate benzyl chloride **9** and 4-hydroxybenzaldehyde (**8**) under basic conditions by using potassium carbonate (K_2CO_3) as a catalyst. Then, the Claisen-Schmidt condensation reaction was performed on appropriate ketones (**11a-c**) and 4-benzyloxybenzaldehyde **10** in alcoholic NaOH at ambient temperature for 24 hours. The precipitate afforded the target chalcone derivatives (**12a-c**).

To confirm the structure of the synthesized chalcones, NMR and ATR-FTIR spectroscopy were used to determine the functional groups and atoms present in the compounds. Chalcones were identified based on the α,β-unsaturated ketone moiety, which is a chemical structure that has two neighboring protons at conjugated C═C double bonds.[10] The compound was anticipated to exhibit doublet signals in the proton-NMR spectra within the chemical shift region of δ 7.00-8.50 ppm, which can be attributed to vicinal coupling. Furthermore, a *trans* configuration is indicated by the coupling constant between 13.0 and 17.0 hertz.[22−24] In the IR spectrum, the carbonyl group of simple aliphatic ketones normally has a strong absorption band in the range of 1720-1708 cm^{-1}. However, for chalcone, the conjugation of C═O will shift the frequency to the lower region due to the delocalization of π electrons (**I**, **II**),[25,26] as illustrated in Scheme 2. In this case, the

Scheme 2. Carbonyl Conjugation to a Carbon−Carbon Double Bond (I, II)

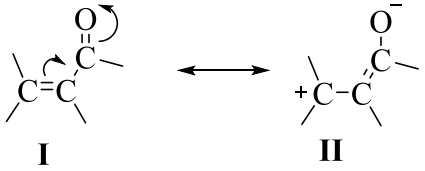

conjugation of C═O with α or β will give rise to absorption in the region 1700-1675 cm^{-1}, whereas C═C will give rise to absorption at 1644-1617 cm^{-1}. The spectral data of the synthesized compounds (**10**) and (**12a-c**) are given in the Supplementary Data File, as shown in **Figures S8-S19**.

2.2. Biological Evaluation. Acetylcholine (ACh) is an essential neurotransmitter that is present in both the central nervous system (CNS) and peripheral nervous system (PNS) of most living organisms. ACh plays the most important role in

https://doi.org/10.1021/acsomega.4c03679
ACS Omega 2024, 9, 32901−32919

Table 1. Molecular Docking Scores and Interaction Modes between Newly Synthesized Chalcones (12a-12c) and AChE (PDB ID: 4EY7)

		Interactions				
		H-bond	Hydrophobic			Electrostatic or Other
Compound	Binding Energy (Kcal/mol)		π-alkyl	π-π T-shape	π-π Stack	C-H bond
12a	-12.0	PHE295, ARG296		TRP286, TRP86, HIS447	TRP286, TRP86, HIS447	TYR341 (π-donor)
12b	-11.6	PHE295	TYR72, TRP286	TYR337, TRP286, TYR341, TRP86	TYR337, TRP286, TYR341, TRP86	
12c	-11.8		TYR72, TRP286	TYR337, TRP286, TYR341, TRP86	TYR337, TRP286, TYR341, TRP86	TYR124

memorization, the learning process and mood control in the CNS. In the PNS, ACh acts as a division of the somatic nervous system and is a main neurotransmitter in the autonomic nervous system and is closely associated with the cardiovascular system of the body.[27] The synthesized derivatives (**12a-c**) were assessed for AChE inhibition activity using spectroscopic Ellman's protocol with acetylthiocholine iodide (ATCI) as the substrate. Galantamine was used as the standard drug because it is a commercially available AChE inhibitor.[28] The results obtained for AChE inhibition demonstrated that compounds **12a** (82.1%), **12b** (64.4%) and **12c** (84.3%) could inhibit the target enzyme. The percentage of positive compound inhibition was 94.1%.

2.3. Theoretical Studies. *2.3.1. Molecular Docking.* The binding modes and proposed molecular docking scores for the newly synthesized chalcones (**12a-12c**) in the active site of the target enzyme (4EY7) are displayed in Table 1 and Figure 4. An in-depth analysis of the findings indicated that compound derivatives **12a**−**12c** exhibited binding free energy (ΔGb) values ranging from -11.6 to -12.0 kcal/mol, whereas the control compound (galantamine) exhibited a value of -7.0 kcal/mol. As illustrated in Figure 4, the chalcone moieties occupied the catalytic anionic site (CAS) of the enzyme *via* hydrogen bonds (HBs) between carbonyl oxygen, benzyloxy and phenyl rings, with residue and binding energies of -12.0, -11.6 and -11.8 kcal/mol, respectively, corresponding to compounds **12a-c**. Target compounds **12a** and **12b** formed (HBs) with PHE295 and more HBs with ARG296 for **12a** derivatives. Both compounds **12b** and **12c** form π-alkyl interactions with TYR72 and TRP286; π-π T-shaped hydrophobic interactions with TYR337, TRP286, TYR341, and TRP86; and π-π stacking interactions with the same residues, TYR337, TRP286, TYR341 and TRP86, where compound **12c** forms HBs with TYR124. In the case of compound **12a**, an interaction with TYR341 occurred (π-donor), which was another interaction involving a π-π stacking and π-π T-shaped interaction with the TRP286, TRP86, and HIS447 amino acid residues. A meticulous examination of the patterns of binding energy and binding sites between the AChE enzyme and the series of interest **12a-12c** indicated that both **12a** and **12c** chalcone compounds could be good candidates for AChE inhibitors. In our upcoming discussion, we will examine the stability of complexes containing both **12a** and **12c**. This analysis will be conducted through molecular dynamics simulation coupled with free energy calculations.

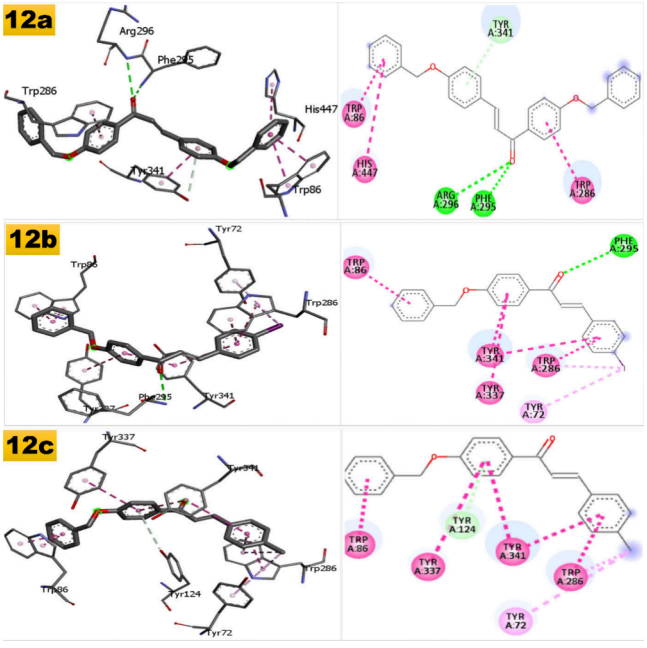

Figure 4. Proposed binding mode of newly synthesized compounds (**12a-12c**) docked in the active site of the enzyme (PDB ID: 4EY7) (2D and 3D compound-receptor interactions).

2.3.2. Molecular Dynamics Simulation and System Stability. The molecular interactions and the water solvent conditions around the protein influence the conformational stability of the protein-compound interaction. The pose with the highest binding affinity, obtained from docking simulations (**12a** and **12c**), was used as the starting structure. As well as, in order to forecast its stability and interaction, a molecular dynamic simulation was employed.[29,30] Therefore, a long-range MD simulation of 100 ns was performed on the docked complexes to investigate the dynamics, conformational stability, and structural stability of the protein-compound complexes. In this investigation, the root-mean-square deviation (RMSD) was employed to assess the stability of the systems throughout the 100 ns simulations. A RMSD value range of less than 5.0 Å was deemed the most acceptable, given that a reduced RMSD value signifies enhanced system stability.[31] For all frames of the AChE protein, compound protein complex systems and compounds **12a** or **12c** are shown in Figure 5. In addition, **b**, the average RMSD values were 2.19, 1.7 and 2.21 Å for the **12c** complex and 2.39, 2.28 and 2.51 Å for the **12a** complex. The standard deviations of the average RMSD values were 0.21, 0.30 and 0.21 Å for the case **12c** complex and 0.28, 0.37 and 0.30 Å, respectively, for the **12a** complex.

The results indicated that the **12c** complex system attained a more stable conformation than the other **12a** complex systems

https://doi.org/10.1021/acsomega.4c03679
ACS Omega 2024, 9, 32901−32919

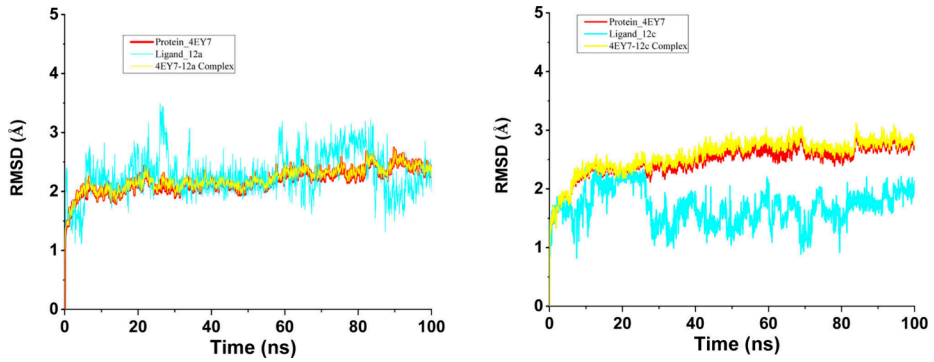

Figure 5. Root mean square deviation (RMSD) of the solvated protein backbone, the compounds (**12a** and **12c**) and the receptor-compound complex.

examined. To analyze the behavior of the residue and its correlation with the compound during MD simulation, it is necessary to assess the flexibility of the protein structure when the compound binds to it.[31] Protein residue variations were evaluated utilizing the root-mean-square fluctuation (RMSF) method to ascertain the influence of inhibitor binding to the relevant targets throughout 100 ns of simulation. The average RMSF values that were computed for the systems involving the **12a**-AChE complex and the **12c**-AChE complex to protein systems were 1.15 and 1.05 Å, respectively. Figure 6 depicts

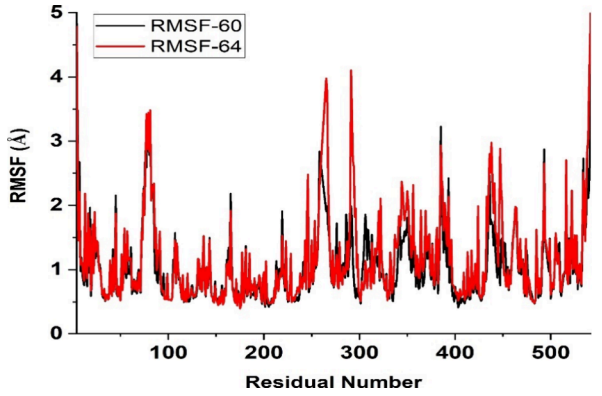

Figure 6. Root mean square fluctuations (RMSFs) of the solvated protein backbone and the complex of compounds **12a** and **12c**.

the overall residue fluctuations of several systems of the **12a** and **12c** protein complexes. These values indicate that the inhibition of the **12c**-AChE protein complex system is lower than the inhibition of other systems. This finding suggests that the complex is more stable.

The number of hydrogen bond interactions between the protein and the compounds was determined by computing the angle cutoff at 10 degrees and the rcut at 3.0 Å. These values were subsequently plotted against a time of 100 ns, as depicted in Figures S1a and b. The average number of hydrogen bonds per time period for the **12a** and **12c** complexes, respectively, was determined to be 1.06 and 0.9 Å, respectively, based on calculations of hydrogen bonds.

Compound−protein interactions substantially increased the number of hydrogen bonds per trajectory analysis from 1 to 4 HBs according to the overall analysis. The observed values indicate that the conformation of the system **12a** complex became more stable than that of the other system **12c** complex, as determined through hydrogen bond formation interactions.

The parameter that indicates the stability of the protein and its structural compactness during simulations is the radius of gyration (R_g). The average Rg values for all frames of the AChE protein, compound **12a** or **12c**, and compound protein complex systems are depicted in Figure S2a and b. The values for the **12a** complex were 2.32, 0.65, and 2.31 Å, respectively, while those for the **12c** complex were 02.31, 0.54 and 2.31 nm, respectively. The average RMSD values were accompanied by standard deviations of 0.01, 0.03, and 0.01 nm for both the **12a** and **12c** complexes. The R_g values of both protein complexes were found to be almost the same as those of the rigid complexes.

The solvent-accessible surface area (SASA) of the protein was calculated during MD simulation under compound-bound conditions. The SASA values changed due to the binding of the compound to the protein, as shown in Figures S3a and b. As demonstrated by the analysis, the folding states of the proteins and their stability upon compound binding occurred in the case of the **12c**-protein complex rather than in the case of the **12a**-protein complex due to the compound geometry, as shown in the results. The average SASA was 6.44 nm for the **12c** complex, whereas for the **12a** complex, the SASA was 7.8 nm; additionally, the protein and its complexes underwent a minor change. Over the course of the 100 ns simulation, the mean distance between the center of mass of the protein residues and compound **12a** or **12c** is illustrated in Figure 7. As a function of time, complex **12a** is shorter than complex **12c** is, which maintains a proximity of approximately 1.36 and 1.80

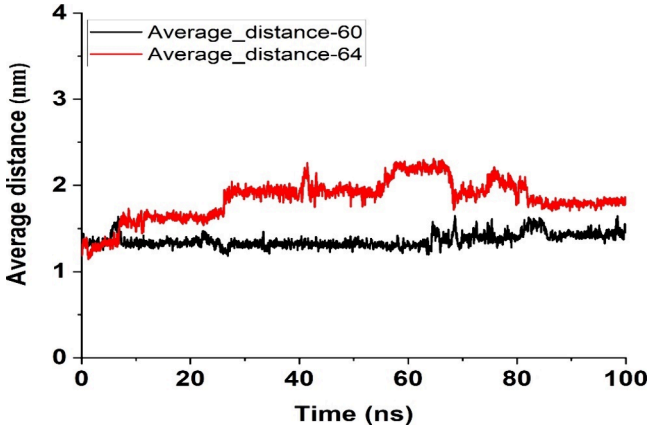

Figure 7. Average distance between the compounds vs. center of mass analysis for protein-compounds (**12a** and **12c**).

https://doi.org/10.1021/acsomega.4c03679
ACS Omega 2024, 9, 32901−32919

Table 2. Summary of the Free Energies of Binding MM/PBSA and MM/GBSA Calculated for the Top Docked Chalcone Derivatives (12a and 12c) with the Target Enzyme (PDB ID: 4EY7)

				MM-GBSA				MM-PBSA			
complex	ΔE_{VDW}	ΔE_{ELE}	ΔG_{GAS}	ΔE_{GB}	ΔE_{SURF}	ΔG_{SOL}	ΔG_{Bin}	ΔE_{PB}	ΔE_{NPolar}	ΔG_{SOL}	ΔG_{Bin}
12a	-47.29	-11.46	-58.75	36.16	-6.44	29.73	**-29.02**	46.99	-5.3	41.69	**-17.06**
12c	-37.66	-8.15	-45.81	20.95	-5.02	15.93	**-29.88**	28.93	-4.08	24.85	**-20.96**

Table 3. Physicochemical Property Analysis and QSAR Properties of Compounds 12a-12c toward the Target Enzyme (PDB ID: 4EY7) for Drug Design

Compd	Polarizability (A^3)	Refractivity (A^3)	Vol (A^3)	Surface Area (Grid) A^2	HE (kcal/mol)	Log *P*	MW (DA)	TPSA (Å)	HBA	HBD	Fraction Csp3
12a	49.76	129.03	1280.21	760.09	-7.93	6.72	420.51	35.53	3	0	0.07
12b	42.65	110.36	1066.21	647.53	-5.33	6.46	440.28	26.30	2	6	0.05
12c	39.46	102.99	1036.17	630.35	-4.5	5.67	328.41	26.30	2	6	0.09

nm, respectively. The stability, conformation, and motion of chalcone **12c** are reflected in this. As shown in Figures S4a and b, contact frequency (CF) analysis was conducted to estimate the binding between compound **12a** or **12c** and AChE complexes. The contactFreq.tcl module on VMD was utilized, and a cutoff of 4 Å was applied to the analysis. In the simulated 12a complex case study, the amino acid residues listed below demonstrated significantly higher CF values, reaching a remarkable 99.15%: TRP86, GLY121, TYR124, SER125, GLY126, TYR133, TRP286, PHE297, TYR337, PHE338 and TYR341. Good contact surfaces exist between the **12c** complex and the protein pocket. The simulation investigation revealed that amino acid residues had elevated CF values, amounting to 97.7%: TYR71, LEU76, TYR124, TRP286, HSD287, SER293, GLN291, PHE238, TYR341 and GLY342.

2.3.3. Binding Free Energy of MM/GBSA and MM-PBSA. The molecular mechanics energy technique (MM/GBSA and MM/PBSA) is a widely used approach for determining the free binding energies of small molecules to biological macromolecules. The GBSA integrates the generalized Born and surface area continuum solvation models. In contrast, the one-average molecular mechanics Poisson-Boltzmann surface area (MM-PBSA) method, which analyzes ensembles of the initial and final states to compute the free energy of binding,[32,33] operates path-independently; therefore, the efficacy of MM-PBSA surpasses that of MMGBSA. Both strategies may exhibit greater reliability than docking scores. Both techniques may be more reliable than docking score.[30,31] The computed binding free energy of the simulated complex was used to confirm the expected inhibitory affinity of **12a** and **12c** for the AChE receptor complex, as determined by docking simulation studies, the results of which are given in Table 2. The binding free energies were computed by utilizing snapshots obtained from the trajectories of the system during a duration of 100 ns; afterwards, the gmx_MMPBSA tool was executed using GROMACS files and the AMBER tool MMPBSA.py.[34]

Table 2 displays the reported computed energy solvation components, with large negative values signifying advantageous interactions. The **12c** complex binding free energy was computed to be -29.88 or -20.96 kcal/mol for mmgbsa and mmpbsa, respectively, and for the **12a** complex, it was calculated to be -29.02 or -17.06 kcal/mol for mmgbsa and mmpbsa, respectively. Upon careful examination of the individual energy contributions, it became evident that the van der Waal electrostatic energy decreased (−37.66, −8.15 kcal/mol) in the **12c** complex and in the **12a** complex -47.29 and -11.46, respectively. Finally, other energy components have considerable and moderate values for both complexes. Binding free energy analysis revealed that the **12c**-4EY7 complex is more stable than the other complex, with differences ranging from 0.8 to 3.9 kcal/mol, which indicates that it is highly amenable to inhibition by AChE.

2.3.4. Structural Activity Relationships (SAR). The present investigation utilized HyperChem (v8.0.7) to compute and analyze the physicochemical properties, such as hydration energy (HE), polarizability (Pol), molar volume (V), surface area grid (SAG) and molar refractivity (MR), of the synthesized compounds (**12a-12c**), as shown in Table 3. The compound's molecular polarizability (Pol) was assessed by assessing the effectiveness of its electronic system in regulating itself when exposed to an external electric field of light. Molecular polarizability is of the utmost importance because it is utilized to simulate bioactivities and a variety of compound characteristics.[35] The molecular polarizability of a molecule is governed primarily by its volume, which governs processes such as intestinal absorption and blood−brain barrier permeability. Therefore, the molecular volume must be utilized to simulate the molecular properties and bioactivities in QSAR investigations. Another SAR parameter is molar refractivity (MR), which is influenced by the spatial arrangement of the phenyl ring in the compounds under study. The spatial arrangement is of utmost importance because it is essential for comprehending the manner in which medication molecules interact with biological receptors. The London dispersion force plays a significant role in the interaction between drug molecules and receptors and is another factor that affects molar refractivity, in addition to its correlation with molecular volume.

Molecular refractivity, surface area grid and polarizability data are frequently correlated with the volume (volume) and molecular weight (MW) of proposed chalcones, as shown in Table 3. Compound **12a** had the highest volume (1280.21 $Å^3$), highest surface area (760.09 $Å^3$), highest MW (420.51 amu), highest polarizability (49.76 $Å^3$), and highest refractivity (129.03 $Å^3$). In contrast, compound **12c** exhibited diminished values across all descriptors, including MW328.41 amu. Polarizability = 39.46 $Å^3$, molecular volume = 1036.17 $Å^3$, surface area = 630.35 $Å^2$ and refractivity =102.99 $Å^3$. Based on the results presented in Table 3, the other chalcones (**12b**) are intermediate between the maximum and minimum chalcones, where the MW, polarizability, molecular volume, surface area

https://doi.org/10.1021/acsomega.4c03679
ACS Omega 2024, 9, 32901−32919

Table 4. Pharmacokinetic Properties of the Synthesized Chalcone Hybrids (12a-c)

				Metabolic enzymes Inhibitors					
Compd	GI Absorption	BBB Permeant	p-gp Substrate	CYP1A2	CYP2C19	CYP2C9	CYP2D6	CYP3A4	Skin P Log Kp (cm/s)
12a	High	No	Yes	No	Yes	No	No	Yes	-4.60
12b	High	Yes	Yes	Yes	Yes	Yes	No	Yes	-5.29
12c	High	Yes	Yes	Yes	Yes	Yes	No	Yes	-4.82

Table 5. Lipophilic and Water Solubility Properties of the Synthesized Chalcone Compounds (12a-c)

	Log S (ESOL)			Log S (Ali)			Log S (SILICOS-IT)			Lipophilicity
Compd	ESOL	Solubility mg/mL	Class	Ali	Solubility mg/mL	Class	Silicos-IT	Solubility mg/mL	Class	Consensus Log $P_{0/w}$
12a	-6.19	2.69e-04	Poorly Soluble	-6.53	1.23e-04	Poorly Soluble	-10.18	2.78e-08	Insoluble	5.71
12b	-5.98	4.58e-04	Moderately soluble	-5.50	1.39e-03	Moderately Soluble	-8.45	1.57e-06	Poorly Soluble	5.16
12c	-5.11	2.57e-03	Moderately soluble	-5.20	2.08e-03	Moderately Soluble	-7.98	3.47e-06	Poorly Soluble	4.85

grid, and refractivity are 440.28 amu, 42.65 Å^3, 1066.21 Å^3, 647.53 Å^2, and 110.36 Å^3, respectively.

2.3.4.1. In Silico-Predicted Physicochemical and Pharmacokinetic Properties of Compounds ***12a-c.*** The results presented in Table 3 demonstrate that as the hydrophobicity increases, the hydration energy decreases. The stability of molecular conformations in aqueous solutions is determined by the hydration energy.[36,37] An increase or decrease in the number of hydrogen bonds (donors and acceptors) influences the variation in the hydration energy. Table 3 presents the absolute values of hydration energy in the following order: **12c** < **12b**< **12a** with values of (-4.5, - 5.33, and -7.93 kcal/mol) and characterized by hydrogen bonds (acceptors and donors).

A significant factor in determining numerous ADME properties is lipophilicity. The Log P quantifies the distribution of drug molecules between the aqueous environment outside the cell membrane and the lipid composition of the cell membrane. This means that compounds possessing a lower Log P value exhibit greater polarity and reduced permeability across lipid bilayers. Conversely, compounds characterized by a greater Log P value exhibit reduced polarity and inferior solubility in water.[38] All the compounds ranged from 5.7-6.7 *log P* values of solubility. Moreover, the log *P* values of compounds **12c** < **12b**< **12a** are outside the range of optimal values (0 < *Log P* < 5).[39] Based on their favorable biological activity, it can be inferred that these chalcone compounds necessitate the deposition of a drug delivery carrier onto the surface of a nanomaterial possessing specific properties to improve oral bioavailability, which is very near optimal, as shown in Table 3. The pharmacokinetic properties of the studied compounds (Table 4) revealed that the compounds exhibited high gastrointestinal absorption; this score indicates rapid digestion and absorption of synthesized compounds in the small intestine. Another very important prediction is blood−brain barrier permeation, which is crucial for treating Alzheimer's disease and is exhibited by compounds **12b** and **12c** but not by compound **12a**. These findings suggest that compounds **12a** and **12b** can penetrate the central nervous system (CNS), making them useful for treating infections such as AD.

Permeability glycoprotein (P-gp) acts as a xenobiotic barrier to the central nervous system. Table 4 reveals that the synthesized compounds are effective P-gp substrates and xenobiotic inhibitors. Table 4 reveals that the metabolism of some metabolic enzymes is inhibited, while that of others is successful. Another monumental property is the Lipinski rule of five, which includes several sets of rules and guidelines that are all scored by the synthesized compounds.

The predicted water solubilities indicate that compounds **12b** and **12c** are more soluble in aqueous environments than compound **12a**, which is insoluble in the SILICOS-IT class (Table 5). Additionally, the predicted conditional Log P $_{0/w}$ values of the three synthesized compounds fall within the range of 4.87 to 5.71, which is an indication that the compounds can have good ADME properties in the lipid region (Table 5).

2.3.5. Density Functional Theory (DFT). 2.3.5.1. Molecular Orbital Calculations. Using spectroscopic data and elemental analysis, natural charges, molecular electrostatic potential maps, the natural population of the nucleus of the proposed derivatives, the optimized geometrical parameters (bond lengths, bond angles, and dihedral angles), the energetics of the ground state and the reactivity descriptors of the studied molecules were computed and analyzed.

2.3.5.2. Ground-State Geometric Parameters. Table 6 and Figure 8 present the optimized geometry, numbering system, vector of the dipole moment, bond length, bond angle and dihedral angle of chalcone derivatives **12a-12c** as benchmarks for this work. For the selected geometrical parameters, we decided to compare the gas-phase wB97XD/6-311++G(d,p) estimates to the available crystal data X-ray structure of 4-bromo-4′-methoxy-chalcone (ref. CCDC 1199470).[40] The calculated mean absolute errors (MAEs) for the selected angles and bond lengths of the chalcone nucleus are presented in Table S1. A close inspection revealed that MAEs for bond length vary from 0.0 to 0.2 Å; for dihedral angles in long-range corrected hybrid functionals (wB97XD), MAEs range from 0.0 to 2.83 degrees; and for bond angles, MAEs range from 0.0 to 2.18 degrees, which provide complete reducibility for bond length and angle prediction, with empirical findings concerning the duration of computer processes and power uses. As a consequence, the wB97XD/6-311++G level of theory is chosen for all calculations and geometry optimizations. Among the compounds (**12a-12c**), a significant proportion of the computed bond lengths are underestimated, varying in percentage from 0.0 to 5.1% for C12-O15, C16-C21, C18-C19 and C26-O27, and overestimations occur, with percentages varying from 1.1 to 12.1% for the other bond lengths. In general, there was a minor variation within the region of the derivative group. Analysis of the dihedral angles presented in Table 4 reveals that the majority of the molecules exhibit

https://doi.org/10.1021/acsomega.4c03679
ACS Omega 2024, 9, 32901−32919

Table 6. Selected Bond Length (Å), Bond Angles and Dihedral Angles (Degree) of the Compounds (12a-12c)[a]

	12a	12b	12c		12a	12b	12c
R(C1,C2)	1.393	1.394	1.394	A(C12,O15,C16)	118.4	118.6	118.5
R(C1,C6)	1.392	1.391	1.392	A(O15,C16,C17)	124.6	124.6	124.6
R(C1,C12)	1.502	1.502	1.502	A(O15,C16,C21)	115.7	115.6	115.7
R(C2,C3)	1.389	1.388	1.389	A(C17,C16,C21)	119.8	119.8	119.7
R(C3,C4)	1.391	1.391	1.391	A(C16,C17,C18)	119.5	119.5	119.5
R(C4,C5)	1.390	1.389	1.390	A(C17,C18,C19)	121.2	121.2	121.2
R(C5,C6)	1.390	1.391	1.390	A(C18,C19,C20)	118.5	118.5	118.5
R(C6,H7)	1.086	1.085	1.086	A(C18,C19,C26)	123.0	123.0	123.0
R(C12,O15)	1.423	1.424	1.423	A(C20,C19,C26)	118.4	118.3	118.4
R(O15,C16)	1.352	1.351	1.352	A(C19,C20,C21)	120.9	120.9	120.9
R(C16,C17)	1.394	1.394	1.394	A(C16,C21,C20)	120.0	120.1	120.1
R(C16,C21)	1.400	1.400	1.400	A(C19,C26,O27)	120.4	120.7	120.4
R(C17,C18)	1.392	1.392	1.392	A(C19,C26,C28)	120.5	120.5	120.5
R(C18,C19)	1.391	1.392	1.391	A(O27,C26,C28)	119.2	118.8	119.1
R(C19,C20)	1.401	1.401	1.401	A(C26,C28,C30)	124.8	124.5	124.4
R(C19,C26)	1.495	1.493	1.494	A(C28,C30,C32)	126.9	126.8	127.1
R(C20,C21)	1.378	1.377	1.378	A(C30,C32,C33)	119.1	118.8	118.8
R(C20,H23)	1.084	1.084	1.084	A(C30,C32,C37)	123.4	123.1	123.3
R(C26,O27)	1.218	1.216	1.217	A(C33,C32,C37)	117.6	118.1	117.8
R(C26,C28)	1.482	1.486	1.484	A(C32,C33,C34)	121.6	121.4	121.2
R(C28,C30)	1.339	1.337	1.338	A(C33,C34,C35)	119.9	119.4	120.9
R(C30,H31)	1.088	1.087	1.088	A(C34,C35,A40)	115.9	156.4	121.3
R(C30,C32)	1.466	1.469	1.467	A(C36,C35,A40)	124.6	83.7	120.8
R(C32,C33)	1.402	1.397	1.397	D(C6,C1,C2,C3)	-0.1	0.0	0.0
R(C32,C37)	1.395	1.399	1.400	D(C12,C1,C2,C3)	-179.1	-179.3	-179.0
R(C33,C34)	1.381	1.388	1.388	D(C2,C1,C12,O15)	84.0	76.0	81.0
R(C34,C35)	1.396	1.389	1.392	D(C6,C1,C12,O15)	-95.0	-103.2	-98.0
R(C35,C36)	1.396	1.083	1.398	D(C1,C12,O15,C16)	179.8	-178.7	179.2
R(C35,A40)	1.353	1.393	1.505	D(C12,O15,C16,C17)	0.6	-1.3	-0.1
R(C36,C37)	1.388	2.090	1.384	D(C12,O15,C16,C21)	-179.7	179.1	-179.6
R(C33,Cl,O42)				D(O15,C16,C17,C18)	-179.2	179.5	179.8
R(C33,Cl,O41)				D(C21,C16,C17,C18)	1.1	-1.0	-0.7
R(O40,43)	1.418			D(C18,C19,C26,O27)	147.8	-149.8	-147.8
R(O42,41,C43)				D(C18,C19,C26,C28)	-33.0	31.2	33.3
A(C2,C1,C6)	119.2	119.2	119.2	D(C20,C19,C26,O27)	-28.6	26.6	28.4
A(C2,C1,C12)	120.3	120.1	120.3	D(C19,C26,C28,C30)	-28.6	30.7	29.7
A(C6,C1,C12)	120.5	120.7	120.5	D(O27,C26,C28,C30)	150.5	-148.4	-149.3
A(C1,C2,C3)	120.5	120.4	120.5	D(C26,C28,C30,C32)	-174.8	174.8	173.9
A(C2,C3,C4)	120.0	120.0	120.0	D(C28,C30,C32,C33)	-171.8	-174.1	-175.6
A(C3,C4,C5)	119.9	119.9	119.9	D(C28,C30,C32,C37)	7.7	6.3	4.2
A(C4,C5,C6)	120.0	119.9	120.0	D(C30,C32,C33,C34)	178.5	-179.9	179.6
A(C1,C6,C5)	120.5	120.5	120.5	D(C33,C34,C35,H40)	-179.6	0.0	178.9
A(C1,C12,O15)	108.2	108.2	108.2	D(H40,C35,C36,C37)	179.4	-0.1	-179.0

[a]A= H, Cl, Br, F, O, O, N, I, C, H, H, H or H means different atom in derivatives series, respectively. Values are mean ± SD triplicate assays.

planar geometry, with the exception of the benzyloxy moiety, which is out of plane in all the target compounds (**12a-12c**), ranging from 26.0 to 33.5 degrees for dihedral angles.

The bond angles computed in Table 6 range from 108.0 to 124.0 degrees, which are favorable compared to those of a regular sp^3 hybridization methoxy group and sp^2 hybridization for the rest of the molecule inside the benzene rings and *trans*-ethylene group geometry, respectively. Furthermore, the optimized geometries of chalcones **12a-12c**, numbering systems, dipole moment vectors, bond lengths, bond angles and dihedral angles are presented in Table 6 and Figure 8 and were calculated at wB97XD/6-311++G(d,p), the best level of theory. The target molecules contained C, O aromatic and nonaromatic rings with single-double resonances with bond lengths varying from 1.3 to 1.5 Å and bond angles varying from 115.6 to 126.0 degrees, which are correlated with the basic concepts of hybridization of molecular orbitals. At the dihedral angles, the benzyl moieties out of plane D (C2, C1, C12, O15) and D (C6, C1, C12, O15) are 76.0-98.0 degrees, respectively. The proposed chalcone derivatives are very similar in terms of the geometrical structure and planarity of the chalcone group, as indicated by the consistency of the bond length, angle and dihedral angle; however, the changes in the C40 derivative group are also similar to those of the regular sp^2 and sp^3 hybridization geometries.

2.3.5.3. Natural Charges and the Natural Population. The electronic structures of the target compounds (**12a-12c**) were subjected to natural charge analysis, which provided a precise depiction of the electron distribution across different subshells of their atomic orbitals. Charge analysis of all the compounds

https://doi.org/10.1021/acsomega.4c03679
ACS Omega 2024, 9, 32901−32919

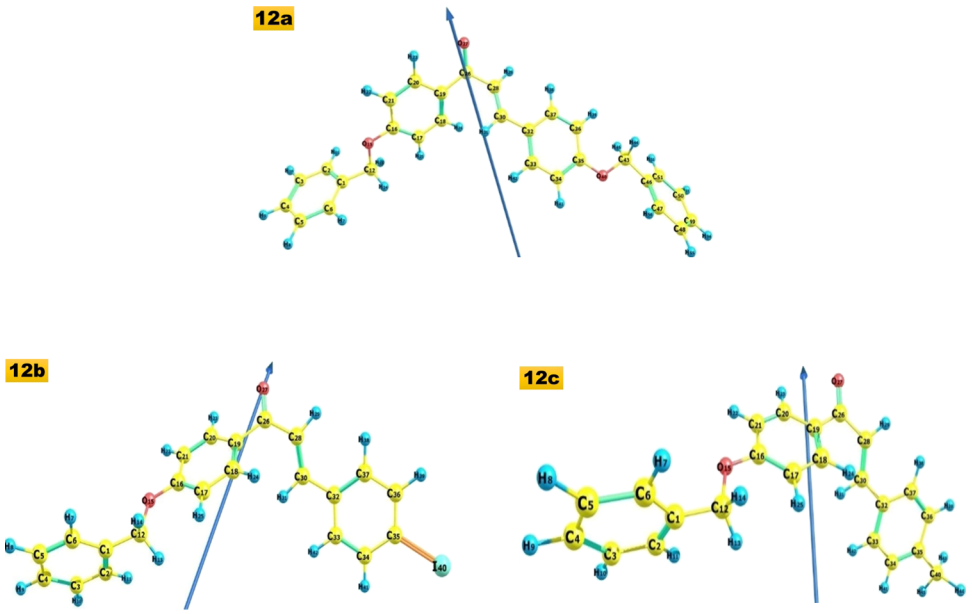

Figure 8. Optimized geometry, numbering system, and vector of dipole moments of the compounds (**12a-12c**).

was conducted using the wB97XD/6-311++G(d,p) level of calculation, and the results are shown in Table 7. In Table 7, the most electronegative charges for **12a-12c** are attributed to O27, O15, C17, C28, C21 and C40 in the case of compounds **12a** and **12c**, respectively, from -0.598e to -**0.256e**. From an electrostatic perspective, these highly electronegative atoms tend to possess electrons. Nevertheless, the atoms with the highest electropositivity for chalcones (**12a-12c**), such as C26, C16, H23, and H22 for all the series and C35 in compound **12a**, ranged from +0.531e to +0.225e, which are inclined to have active sites accepting electrons. A minor alteration in the natural charge occurs as one transition from **12a** to **12c**, following the identical sequence pattern of electrostatic mapping with ordering. An extensive investigation of the natural charge patterns of the three active target compounds is very helpful for gaining a deeper understanding of the important interactions between these active sites and biological receptors. Understanding the critical interactions that occur between hybrid chalcones and biological receptors of AChE is greatly facilitated by the natural charge pattern of chalcones, which allows examination of cytotoxic activity.

Table 7. Natural Charge of Selected Atoms of Newly Synthesized Compounds 12a-12c[a]

	12a	12b	12c
C1	-0.063	-0.064	-0.063
C2	-0.186	-0.185	-0.186
C3	-0.201	-0.200	-0.201
C4	-0.199	-0.199	-0.199
C5	-0.202	-0.201	-0.201
C6	-0.188	-0.189	-0.188
C12	-0.041	-0.040	-0.041
O15	-0.543	-0.542	-0.543
C16	0.350	0.353	0.351
C17	-0.312	-0.312	-0.312
C18	-0.147	-0.145	-0.146
C19	-0.182	-0.187	-0.184
C20	-0.139	-0.137	-0.139
C21	-0.245	-0.244	-0.245
H22	0.225	0.226	0.225
H23	0.230	0.231	0.230
C26	0.531	0.531	0.531
O27	-0.566	-0.560	-0.564
C28	-0.281	-0.256	-0.275
C30	-0.118	-0.143	-0.122
C32	-0.136	-0.089	-0.107
C33	-0.154	-0.163	-0.166
C34	-0.244	-0.227	-0.207
C35	0.344	-0.194	-0.016
C36	-0.297	-0.222	-0.201
C37	-0.141	-0.162	-0.165
C40	-0.547	0.180	-0.598
C43	-0.037		
C46	-0.059		
C47	-0.192		

[a]A=H, Cl, Br, F, O, O, N, I, C, H, H, H or H means different atom in derivatives series; values are mean ± SD triplicate assays.

2.3.5.4. Frontier Molecular Orbitals (FMOs) Analysis. According to the information provided in Table 8, compound **12c** exhibited superior stability and lower reactivity than did the other potential chalcones, with an energy gap of 8.06 eV; in contrast, chalcone **12a** (ΔEg = 7.83 eV) exhibited the greatest reactivity and the least stability.[41,42] The rest of the active forms of **12b** exhibited an energy gap of 7.85 eV. Therefore, calculations of these parameters, including A (electron affinity) and I (potential ionization), are crucial in determining the global reactivity descriptors. The one-electron orbital energies of the HOMO and LUMO are associated with the I and A parameters. According to the results, chalcone **12b** had the highest I value (8.41 eV), A value (0.56 eV) and electronegativity (X) (4.49 eV). The I, A and X values of the other chalcones exhibit the same pattern (**12c>12a**). Here, derivatives **12c** and **12a** are anticipated to be the most promising candidates for interaction with other biological AChE receptors. The HOMO and LUMO isodensity dispersions on the ethylene-phenyl ring, as shown in Figure 9, are nearly identical for all the potential targets, except for

https://doi.org/10.1021/acsomega.4c03679
ACS Omega 2024, 9, 32901−32919

Table 8. Energetic Parameters and Reactivity Indices of Chalcone Derivatives 12a-12c[a]

Parameters	ET, au	EHOMO, au	ELUMO, au	Eg, eV	μ, D	I, eV	A, eV
12a	-1345.06039	-0.29512	-0.00739	7.83	4.99	8.03	0.20
12b	-1296.69366	-0.30918	-0.02072	7.85	4.76	8.41	0.56
12c	-1038.82955	-0.30656	-0.01035	8.06	5.48	8.34	0.28
Parameters	**X, eV**	**η, eV**	**S, eV**	**V, eV**	**ω, eV**		**N, eV**
12a	4.12	3.91	0.13	-4.12	2.16		-3.82
12b	4.49	3.92	0.13	-4.49	2.57		-4.20
12c	4.31	4.03	0.12	-4.31	2.31		-4.13

[a]Values are mean ± SD duplicate assays.

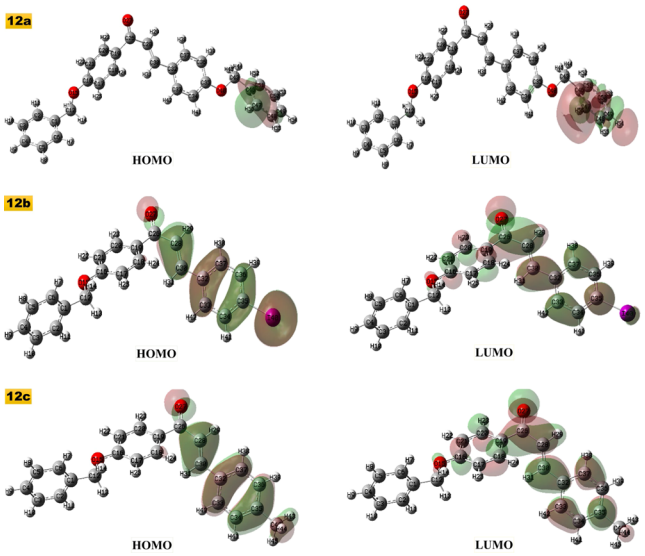

Figure 9. Frontier molecular orbitals of the newly synthesized compounds (**12a-12c**).

chalcone **12a**, which exhibits a somewhat distinct dispersion on the methoxy-phenyl ring. By using the dipole moment vector and the order norm vector, the direction of the electronic charge transfer motion is represented; novel synthesized compounds are ranked in the following order: **12b** < **12a** < **12c**.

2.3.5.5. Global Reactivity Descriptors. Density functional theory (DFT) utilizes the electron density of a chemical system to elucidate fundamental concepts regarding chemical reactivity.[43] The global descriptors obtained by the framework of finite difference approximation were used to address the various qualitative concepts of chemical reactivity, as cited in previous work;[44] these concepts were calculated at the wB97XD/6-311++G (d, p) level of theory. The most formidable challenges in chemistry involve comprehending the essence of chemical interactions and forecasting the chemical reactivity of molecules, atoms, or ions. The reactivity of three target derivatives (**12a-12c**) was investigated in this study. The important reactivity descriptors, which offer insights into the stability and reactivity of chalcones **12a-12c**, are presented in Table 8. Compound **12c** is the most chemically hardest among the others, as it has a maximum value of η = 4.03 eV. In contrast, chalcone **12a** has the lowest value (η = 3.91 eV), indicating its chemical softness and higher reactivity, while another derivative, **12b**, has a chemical hardness of 3.92 eV (η). A fundamental understanding of charge transfer occurring in the ground state of any molecule can be derived from the electronic chemical potential V value. Compound **12b** has the lowest chemical potential (-4.49 eV), compound **12a** has the highest chemical potential (-4.12 eV), and the other compound chalcone **12c** has the lowest value (V = -4.31 eV) (Table 8). The energy changes that occur when a chemical system reaches saturation through the ingress of additional electrons are quantified by a thermodynamic parameter denoted as the electrophilicity index (ω). This approach is extremely useful for determining the chemical reactivity of a system. Compound **12a** is nucleophilic in nature, as indicated in Table 8, with the lowest electrophilicity index value of 2.16 eV. On the other hand, compound **12b** is extremely electrophilic in nature (ω = 2.57 eV). The value of the electrophilicity index (ω) is 2.31 eV for the other chalcone **12c**. Electronegativity (X) refers to an atom's inclination in a covalent bond to attract electrons toward it. Based on the calculated electronegativity values of the synthesized compounds, compound **12b** has the highest electron accepting ability, with an X value of 4.49 eV, and exhibited greater electronegativity than the other chalcones. With regard to the electrophilicity indices, the electronegativity (X) order of other target compounds exhibited the same behavior. Compound **12a** exhibited the highest values of reactivity and softness (0.1277 eV) with regard to global softness (S), while the remaining compounds exhibited an order of **12b**>**12c**.

2.3.5.6. Local Reactivity Descriptor. The principles of local reactivity descriptors have been frequently utilized to investigate the site selectivity and chemical reactivity of a molecule.[45,46] Local descriptors, such as the Fukui function, can be utilized to investigate molecular site selectivity.[47] The equation shown below represents the first derivative of the electronic density $\rho(r)$ with respect to the electron number (N) of a system under the condition of a constant external potential v(r).[48]

$$f(r) = \left(\frac{\partial \rho(r)}{\partial N}\right)_{v(r)} = \frac{1}{2}\left(\frac{\partial \mu}{\partial v(r)}\right)_{v(r)}$$

To determine the active sites, Fukui functions can be computed using the variations in electrical density that occur during a reaction, and the following equation demonstrates that there are three different chemical environments. The Fukui functions $f^{+}(r)$, $f^{-}(r)$ and $f^{0}(r)$ are calculated for three chemical situations using the following equations:[49−51]

$$f^{-}(r) = q_k(N) - q_k(N-1) \approx \rho^{\mathrm{HOMO}}(r) \text{ for electrophilic attack}$$

$$f^{+}(r) = q_k(N+1) - q_k(N) \approx \rho^{\mathrm{LUMO}}(r) \text{ for nucleophilic attack}$$

$$f^{0}(r) = \frac{1}{2}[q_k(N+1) - q_k(N-1)] \approx \frac{1}{2}[\rho^{\mathrm{HOMO}}(r) + \rho^{\mathrm{LUMO}}(r)] \text{ for radical attack}$$

https://doi.org/10.1021/acsomega.4c03679
ACS Omega 2024, 9, 32901−32919

Table 9. Values of the Fukui Functions and Dual Descriptor of Compounds 12a-12c[a]

	12a			12b			12c		
	f(-)	f(+)	Δf	f(-)	f(+)	Δf	f(-)	f(+)	Δf
C1	0.000	-0.001	-0.001	0.000	0.001	0.001	0.000	0.000	0.000
C2	0.000	0.001	0.001	0.000	0.001	0.001	0.000	0.001	0.001
C3	0.000	0.000	0.000	0.000	0.000	0.000	0.000	0.000	0.000
C4	0.000	0.000	0.000	0.000	0.000	0.000	0.000	0.000	0.000
C5	0.000	0.000	0.000	0.000	0.000	0.000	0.000	0.000	0.000
C6	0.000	0.001	0.001	0.000	0.000	0.000	0.000	0.000	0.000
C12	0.000	0.001	0.001	0.000	-0.001	-0.001	0.000	0.000	0.000
O15	0.002	0.005	0.003	0.001	0.004	0.003	0.001	0.005	0.004
C16	0.002	0.029	0.027	0.001	0.022	0.021	0.001	0.025	0.024
C17	0.002	0.001	-0.001	0.003	0.000	-0.003	0.004	0.003	-0.001
C18	0.005	0.024	0.019	0.003	0.016	0.013	0.003	0.025	0.022
C19	0.004	0.022	0.017	-0.001	0.019	0.020	0.001	0.015	0.014
C20	0.000	0.026	0.025	0.001	0.019	0.019	0.000	0.026	0.026
C21	-0.001	0.002	0.002	-0.001	0.001	0.002	-0.002	0.001	0.003
H23	0.000	0.000	0.000	0.000	0.000	0.000	0.000	0.000	0.000
C26	0.000	0.153	0.153	0.002	0.130	0.128	0.002	0.151	0.149
O27	0.042	0.124	0.082	0.037	0.109	0.072	0.063	0.120	0.057
C28	0.179	0.144	-0.035	0.150	0.148	-0.002	0.219	0.140	-0.078
C30	0.051	0.183	0.132	0.048	0.165	0.117	0.076	0.176	0.101
C32	0.180	0.037	-0.143	0.135	0.058	-0.077	0.177	0.046	-0.130
C33	0.038	0.039	0.001	0.048	0.054	0.006	0.073	0.055	-0.019
C34	0.085	0.015	-0.070	0.049	0.032	-0.017	0.052	0.020	-0.032
C35	0.133	0.077	-0.056	0.125	0.096	-0.029	0.179	0.083	-0.097
C36	0.064	0.004	-0.061	0.041	0.013	-0.028	0.042	0.011	-0.031
C37	0.068	0.088	0.019	0.045	0.086	0.041	0.068	0.076	0.008
O40	0.116	0.011	-0.105						
C40							0.012	-0.002	-0.014
I40				0.309	0.018	-0.291			
C43	0.005	-0.002	-0.007						
C46	-0.008	-0.005	0.002						
C47	0.006	0.007	0.001						

[a]Values are mean ± SD triplicate assays.

where $q_k(N)$ is the atomic population on the k_{th} atom for the neutral molecule and $q_k(N+1)$ and $q_k(N-1)$ are the atomic populations on the k_{th} atom for its anionic and cationic species, respectively. Tables 9 and 10 present the descriptor values of all the compounds (**12a-12c**) computed at the wb97xd/6-311++G (d, p) level. Furthermore, understanding the manner in which an atomic site within a molecule may exhibit nucleophilicity or electrophilicity, Labbe et al.[52] proposed an additional dual descriptor ($\Delta f(r)$), which is defined by the equation below:

$$\Delta f(r) = f^+(r) - f^-(r)$$

According to the data presented in Tables 9 and 10, the compounds (**12a-12c**) containing the phosphate moiety exhibit the highest electrophilic reactivity, which is mostly attributed to the following atoms: C28, C32, C35, and C36 and O40, C40 and I40 corresponding to **12a**, **12b** and **12c**, respectively. These compounds are mostly found on the ethylene site attached to the para derivative benzene ring moiety, while the nucleophilic active site in the target compounds (**12a-12c**) is distributed on the chalcone skeleton moiety located on O15, C16, C19, C20, C26, O27 and C30. Additionally, when evaluating the dual descriptor $\Delta f(r)$ for both nucleophilic and electrophilic attacks, along with the philicity indices, identical outcomes can be achieved. The high electronegativity of the atom oxygen redistributed the electron density, as did the insertion of para derivatives. The results presented here are consistent with the analysis of the natural population conducted by calculating the HOMO and LUMO. The generalized philicity concept was introduced by Chattaraj et al. in 2004. They developed a local quantity called philicity coupled with site k in a molecule (f_k^α) using corresponding condensed-to-atom Fukui function variations according to the subsequent equation.[53]

$$\omega_k^\alpha = \omega f_k^\alpha$$

The local filler quantities describing nucleophilic, electrophilic, and radical attacks are represented by α = +, −, and 0, respectively. Based on the given equation, the property with the highest value of ω_k^α is considered the most electrophilic. Furthermore, to define the reactivity of a molecule, Lee et al.[54] proposed different local softness methods.

$$s_k^\alpha = s f_k^\alpha$$

Radical attacks (α = 0) and local quantities of softness for nucleophilic (α = +) and electrophilic (α = -) species are denoted in the equation. To provide a comprehensive analysis, the software package Multiwfn (v. 3.7) utilized CDFT to determine the relative electrophilicity and nucleophilicity, as well as the condensed local softness, local electrophilicity and nucleophilicity index for each atom within the compounds.[55]

https://doi.org/10.1021/acsomega.4c03679
ACS Omega 2024, 9, 32901−32919

Table 10. Values of the Relative Condensed Local Stiffnesses (Hartree*e), Condensed Local Electrophilicity (ElP) and Nucleophilicity (NuP) Indices (e*eV) of Compounds 12a-12c[a]

	12a				12b				12c			
	s+/s-	s-/s+	EIP	NUP	s+/s-	s-/s+	EIP	NUP	s+/s-	s-/s+	EIP	NUP
C1	0.760	1.316	0.006	0.007	0.793	1.260	0.007	0.004	0.827	1.209	0.006	0.005
C2	2.279	0.439	0.000	0.000	1.090	0.918	0.002	0.001	1.325	0.755	0.002	0.001
C3	0.777	1.288	-0.006	-0.008	0.741	1.350	-0.006	-0.004	0.773	1.293	-0.006	-0.005
C4	0.750	1.333	-0.009	-0.011	0.784	1.276	-0.011	-0.007	0.817	1.224	-0.010	-0.008
C5	0.687	1.456	-0.005	-0.007	0.796	1.257	-0.008	-0.005	0.829	1.207	-0.007	-0.006
C6	3.370	0.297	0.001	0.000	0.793	1.261	-0.001	-0.001	0.884	1.131	-0.001	-0.001
C12	0.425	2.353	-0.002	-0.004	0.477	2.095	-0.002	-0.002	0.501	1.997	-0.002	-0.003
O15	0.730	1.370	-0.014	-0.019	0.778	1.286	-0.017	-0.011	0.815	1.227	-0.017	-0.013
C16	0.496	2.015	-0.019	-0.036	0.555	1.803	-0.022	-0.020	0.564	1.774	-0.022	-0.025
C17	0.498	2.007	-0.010	-0.018	0.576	1.737	-0.011	-0.010	0.613	1.632	-0.012	-0.013
C18	-0.304	-3.294	0.004	-0.012	-0.440	-2.273	0.005	-0.005	-0.294	-3.402	0.004	-0.008
C19	1.171	0.854	0.011	0.009	1.021	0.979	0.013	0.007	1.347	0.743	0.014	0.006
C20	0.353	2.833	-0.008	-0.022	0.403	2.479	-0.009	-0.012	0.379	2.642	-0.009	-0.015
C21	0.690	1.450	-0.018	-0.025	0.729	1.371	-0.021	-0.015	0.769	1.300	-0.021	-0.018
H23	0.491	2.037	-0.009	-0.017	0.542	1.844	-0.010	-0.010	0.538	1.858	-0.010	-0.012
C26	0.125	8.026	-0.013	-0.099	0.134	7.473	-0.014	-0.055	0.148	6.745	-0.016	-0.069
O27	0.495	2.022	-0.067	-0.128	0.572	1.749	-0.083	-0.075	0.648	1.544	-0.092	-0.091
C28	1.649	0.607	-0.113	-0.065	1.436	0.696	-0.134	-0.048	1.841	0.543	-0.138	-0.048
C30	0.268	3.733	-0.030	-0.105	0.387	2.581	-0.046	-0.061	0.492	2.033	-0.055	-0.072
C32	6.837	0.146	-0.090	-0.013	2.776	0.360	-0.089	-0.017	4.316	0.232	-0.084	-0.013
C33	1.371	0.730	-0.047	-0.033	1.273	0.785	-0.063	-0.026	1.527	0.655	-0.068	-0.029
C34	2.086	0.480	-0.068	-0.031	1.283	0.780	-0.056	-0.022	1.600	0.625	-0.057	-0.023
C35	1.369	0.731	-0.082	-0.057	1.209	0.827	-0.082	-0.035	1.578	0.634	-0.104	-0.043
C36	2.050	0.488	-0.057	-0.026	1.403	0.713	-0.051	-0.019	1.634	0.612	-0.052	-0.021
C37	1.173	0.853	-0.057	-0.046	1.036	0.966	-0.058	-0.029	1.312	0.762	-0.060	-0.029
O40	3.359	0.298	-0.088	-0.025								
C40									1.517	0.659	-0.029	-0.012
I40					2.191	0.456	-0.351	-0.083				
C43	1.972	0.507	-0.012	-0.006								
C46	1.657	0.604	0.013	0.008								
C47	1.253	0.798	0.003	0.002								

[a]Values are mean ± SD triplicate assays.

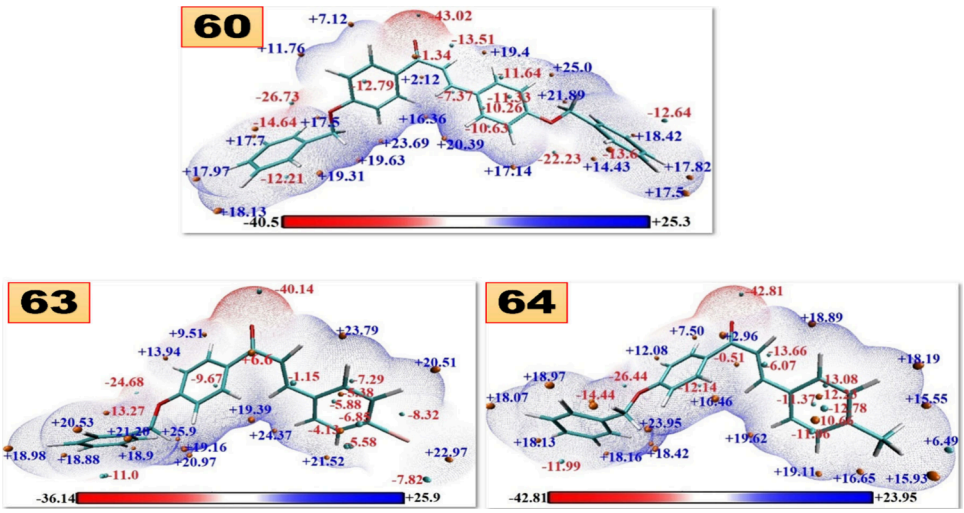

Figure 10. MEP surfaces of the newly synthesized compounds (12a-12c). 12a = 60, 12b = 63, and 12c = 64.

Upon careful examination, it was evident that the centers of the active sites of all the compounds involved electron donation and back-donation processes. These processes align with the frontier orbital and the Fukui functions, as demonstrated by the results presented in Tables 9 and 10. The results of this study indicate that the examined compounds possess multiple active sites, particularly on the chalcone skeleton. This enables them to engage in electron-donating interactions with the surface of the pocket AChE protein. Finally, as demonstrated by the previously mentioned local descriptors, the exper-

https://doi.org/10.1021/acsomega.4c03679
ACS Omega 2024, 9, 32901−32919

imental cytotoxicity of AChE in this study corresponds to the theoretical variation in the efficacy of the compounds.

2.3.5.7. Molecular Electrostatic Potential (MEP). The utilization of electrostatic potential (ESP) on molecular surfaces has emerged as a highly efficient method in numerous domains of chemistry for identifying, analyzing, and comprehending patterns.[56−58] It is associated with electronic density and is a highly accurate descriptor utilized to describe the charge distributions on a molecule, identify regions of varying charges, and determine the most likely sites for hydrogen-bonding interactions and electrophilic and nucleophilic properties.[59] The utilization of electrostatic potentials (ESPs) is critical in the prediction and comprehension of intermolecular interactions.[57] A comprehensive examination of the ESPs of synthesized hybrids is necessary to gain a deeper understanding of the critical interactions that occur between them and biological targets. The electrostatic potential, represented by V(r) (in a.u.), at a specific position r (x, y, z) near the molecule is a computation of the electrostatic energy that a positive unit test charge would encounter at that location. Attractive and repulsive interactions were associated with negative and positive ESPs, respectively. The ESP is the interaction energy between a proton at position r and the electrical charge generated by the nuclei and electrons, as defined by the subsequent equation.

$$V(r) = \sum_{A}^{nuclei} \frac{Z_A}{|R_A - r|} - \int \frac{\rho(r')}{|r - r'|} dr'$$

where ρ (r') denotes the electron density at position r' and ZA and RA represent the charge and position of nucleus A, respectively; all of these values are measured in atomic units.

Figure 10 illustrates the electrostatic potential-mapped surfaces of the studied chalcones **12a-12c**. The quantitative molecular surface analysis module of the Multiwfn package can partition the overall van der Waals surface into multiple fragments. Moreover, this functionality empowers us to analyze the features of the ESP distribution. For compound **12a**, the surface exhibited large negative values for ESP around the carbonyl groups of the chalcone cener (-43.02, -13.51, and -7.37 kcal/mol) and a benzyloxy moiety (-26.73, -14.64 and -12.21 kcal/mol), and an intermediate negative distribution was observed on two phenyl rings of the chalcone arms (-12.79, -11.64, -10.26, and -10.63 kcal/mol) in specific sequence groups of the target compound; additionally, the electron donating ability of the para position C35 attached group increased the global minima rather than did the other two derivatives **12b-12c** of the ESPs around C30=C28-C26=O27, benzyloxy and two phenyl rings of chalcone groups with another benzyloxy in the *para* position, with an increase in the injection of electron density to the overall skeleton of chalcone **12a** (-22.23, -13.6, and -12.64 kcal/mol); however, in cases **12b** and **12c** (Figure 10), the negative decreases in the number of Me derivatives in compound **12c** were attributed to the behavior of small electron donation groups in the sequence (-42.82, -13.66, -6.07 kcal/mol), (-26.44, -14.44 and -11.99 kcal/mol) and (-12.14, (-13.08, -12.25, -12.78, -11.06 for direct phenyl attached) kcal/mol) respectively. Another compound, **12b** (-I), exhibited a negative decrease in intensity as a result of the electron withdrawing group's behavior in the following sequence: (-40.14, +6.6, -1.15 kcal/mol), (-24.68, -13.27, and -11.0 kcal/mol), and (-9.67, (-7.29, -5.38, -5.88, -4.13, and -8.32 kcal/mol, respectively, for direct *para* iodide phenyl attached). The global maxima of the ESPs on the derivative (**12a-12c**) surfaces are located on the carbon with the protons of these derivatives, which vary for **12a** (+7.12, +11.76, +17.7, +17.97, +18.13, +17.5, +19.63, +23.69, +16.36, +20.39, +17.14, +25.0, +18.42 and +17.82 kcal/mol; for **12c** (+7.5, +12.08, 18.97, +18.07, +18.13, +18.16, +18.42, +23.95, +16.46, +20.39, +19.62, +18.89, +18.19 and +15.93 kcal/mol; and for **12b** (+9.51, +13.94,+ 20.53, +18.98, +18.88, +21.20, +18.9, +25.9, +19.39, +23.79, +20.51, +24.37, +21.52 and +22.97 kcal/mol, respectively with the same sequence of chalcone skeletons. Electrostatic or hydrogen bonding mostly occurs between chalcone derivatives and their target receptors for AChE. The occurrence of hydrogen bond interactions and intramolecular charge transfer (ICT) was verified through thorough analysis of these ESP values, suggesting the potential of these materials as therapeutic agents. The results indicate similar findings and patterns to those of the studies conducted on the NBO population and local reactivity descriptors discussed in the preceding section.

3. EXPERIMENTAL SECTION

3.1. Materials and Methods. All chemicals and solvents were obtained from Merck, Sigma-Aldrich, Fisher Scientific, Qrec used without purification. Melting points were measured on Barnstead Electrothermal 9100 melting point apparatus. All reactions were monitored through thin-layer chromatography (TLC) using alumina sheets pre-coated with silica gel 60 F254 (0.2 mm thickness) and the spots were visualized under UV lamp at 254 nm. Infrared (IR) spectra were recorded on Perkin Elmer FT-IR spectrometer using ATR Sampling Accessory. ^{1}H NMR (400 MHz) and ^{13}C NMR (100 MHz) spectra were recorded on Bruker Avance II Spectrometer using TMS as an internal standard. The coupling constants (J) are given in Hertz, and chemical shift values are given in δ (ppm) scales. The HRMS were recorded on Agilent Technologies 6545 Q-TOF LC/MS.

3.2. Preparation of 4-Benzyloxybenzaldehyde (10). Benzyl chloride **9** (0.75 g, 6 mmol), 4-hydroxybenzaldehyde **8** (0.61 g, 5 mmol), 96% ethanol (10 mL) and potassium carbonate (1.35 g, 10 mmol) were added to a round-bottom flask. The mixture was heated under reflux for 6 hours with continuous stirring. After 6 hours, the reaction mixture was left to cool at room temperature before it was poured into ice water, where the precipitates were formed during the process. Vacuum filtration was performed, and the precipitate was washed thoroughly with cold distilled water to obtain the desired product, which was subsequently left to air-dry. Then, the precipitate was purified by recrystallization using ethanol, and thin layer chromatography (TLC) analysis was performed to ensure the completion of the reaction, as shown in Scheme 1. The product was obtained as a light white solid (0.43 g, 40%); m.p.: 71.5-73.5°C; IR, ν_{max} (cm^{-1}): 3037 (sp^2 -CH), 2830 (sp^3 -CH), 1685 (C═O), 1598 and 1454 (aromatic C═C), 1257 (C-O); ^{1}H NMR (400 MHz), δ ppm ($CDCl_3$): 9.92 (1H, s, COH), 7.87 (2H, d, J = 8.8 Hz, H-2′ and H-6′), 7.50-7.40 (5H, m, H-2, H-3, H-4, H-5, H-6), 7.11 (2H, d, J = 8.8 Hz, H-3′ and H-5′), 5.18 (2H, s, H-7); ^{13}C NMR (100 MHz), δ ppm ($CDCl_3$): 190.7 (C═O), 163.8 (C-4′), 136.0 (C-1), 132.0 (C-2′, C-6′), 130.2 (C-1′), 128.7 (C-3,C-5), 128.3 (C-4), 127.5 (C-2, C-6), 115.2 (C-3′, C-5′), 70.2 (C-7).

3.3. General Procedure for the Synthesis of 4-Benzyloxychalcone (12a-c). Substituted aromatic ketone (**11a-c**) (1 mmol) was added to a 50 mL conical flask that

https://doi.org/10.1021/acsomega.4c03679
ACS Omega 2024, 9, 32901−32919

contained a solid of 4-benzyloxybenzaldehyde **10** (0.2122 g, 1 mmol). After that, absolute ethanol (10 mL) was added to dissolve the mixture. Upon complete dissolution, 30% (w/w) sodium hydroxide (NaOH) solution (1 mL) was added dropwise into a continuously stirred solution on a hotplate. The mixture was stirred overnight at room temperature. The resulting solution was allowed to cool to room temperature and was subsequently added to ice water for precipitation. After that, a gravity filtration process was performed, after which the product was washed thoroughly with cold distilled water to obtain the desired product, which was subsequently dried completely in a laboratory oven for a few hours. The recrystallization process was performed using ethanol, and to check the purity of the precipitate, thin layer chromatography (TLC) analysis was performed to ensure the completion of the reaction.

*3.3.1. (E)-1,3-Bis(4-(benzyloxy)phenyl)prop-2-en-1-one (**12a**).* The chalcone (**12a**) was formed as a bright white solid (0.1872 g, 44.52%); m.p.: 145.6− 147.9°C; IR, ν_{max} (cm^{-1}): 3036 (sp^2 -CH), 2946 (sp^3 -CH), 1655 (C═O), 1598 and 1466 (aromatic C═C), 1570 (alkene C═C), 1291 (C-O); ^{1}H NMR (400 MHz), δ ppm ($CDCl_3$): 8.06 (2H, d, J = 8.8 Hz, H-2′, H-6′), 7.80 (1H, d, J = 15.6 Hz, H-β), 7.63 (2H, d, J = 8.8 Hz, H-2 and H-6), 7.50-7.20 (11H, m, H-α, H2″, H-3″, H-4″, H-5″, H-6″, H-2‴, H-3‴, H-4‴, H-5‴, H-6‴), 7.10-7.00, (4H, m, H-3, H-5, H-3′, H-5′), 5.18 (2H, s, H-7‴), 5.14 (2H, s, H-7″); ^{13}C NMR (100 MHz), δ ppm ($CDCl_3$): 188.7 (C═O), 162.5 (C-4′), 160.7 (C-4), 143.7 (C-β), 136.5 (C-1′), 131.7 (C-2′, C-6′), 130.7 (C-2, C-6), 130.0 (C-1), 128.6, 128.2, 128.1, 127.4 (C-1″, C-2″, C-3″, C-4″, C-5″, C-6″, C-1‴, C-2‴, C-3‴, C-4‴, C-5‴, C-6‴), 119.9 (C-α), 115.4 (C-3′, C-5′), 114.7 (C-3, C-5), 70.2 (C-7″, C-7‴). HRMS (ESI): calcd. for $C_{15}H_{12}Br_2O_2S$ $[M + H]^+$ 420.1725, found 420.1694.

*3.3.2. (E)-1-(4-(Benzyloxy)phenyl)-3-(4-iodophenyl)prop-2-en-1-one (**12b**).* The chalcone (**12b**) was formed as a pale orange solid (0.3308 g, 75.13%); m.p.: 151.2− 153.5°C; IR, ν_{max} (cm^{-1}): 3034 (sp^2 =CH), 2942 (sp^3 -CH), 1655 (C═O), 1583 and 1468 (aromatic C═C), 1566 (alkene C═C), 1291 (C-O), 699 (C-I); ^{1}H NMR (300 MHz), δ ppm ($CDCl_3$): 7.88 (2H, d, J = 8.4 Hz, H-2′, H-6′), 7.80 (1H, d, J = 15.6, H-β), 7.75 (2H, d, J = 8.4 Hz, H-2, H-6), 7.61 (2H, d, J = 8.4 Hz, H-2″and H-6″), 7.50-7.30 (6H, m, H-3, H-5, H-3″, H-4″, H-5″, H-α), 7.03 (2H, d, J = 8.4 Hz, H-3′, H-5′), 5.13 (2H, s, H-7″); ^{13}C NMR (75 MHz), δ ppm ($CDCl_3$): 189.7 (C═O), 161.0 (C-4′), 145.3 (C-β), 137.7 (C-2′, C-6′), 136.3 (C-1′), 130.4 (C-2, C-6), 130.3 (C-1), 129.9, 128.7, 128.3, 127.6 (C-1″, C-2″, C-3″, C-4″, C-5″, C-6″), 119.2 (C-α), 115.3 (C-3′, C-5′),100.4 (C-3, C-4, C-5), 70.1 (C-7″). HRMS (ESI): calcd. for $C_{15}H_{12}Br_2O_2S$ $[M + H]^+$ 440.0342, found 440.0273.

*3.3.3. (E)-1-(4-(Benzyloxy)phenyl)-3-(p-tolyl)prop-2-en-1-one (**12c**).* The chalcone (**12c**) was obtained as light green solid (0.100 g, 30.45%); m.p.: 118.2− 120.5°C; IR, ν_{max} (cm^{-1}): 3033 (sp^2 -CH), 2916 (sp^3 -CH), 1655 (C═O), 1604 and 1456 (aromatic C═C), 1586 (alkene C═C), 1295 (C-O); ^{1}H NMR (300 MHz), δ ppm ($CDCl_3$): 7.94 (2H, d, J = 8.1 Hz, H-2′, H-6′), 7.79 (1H, d, J = 15.9 Hz, H-β), 7.62 (2H, d, J = 9.0 Hz, H-2 and H-6), 7.50-7.20 (8H, m, H-3, H-5, H-2″, H-3″, H-4″, H-5″, H-6″, H-α), 7.02, (2H, J = 9.0 Hz, H-3′ and H-5′), 5.13 (2H, s, H-7″), 2.45 (3H, s, H-7); ^{13}C NMR (75 MHz), δ ppm ($CDCl_3$): 190.1 (C═O), 160.7 (C-4′), 144.2 (C-β), 143.4 (C-2′, C-6′), 136.4 (C-1′), 135.9 (C-2, C-6), 130.2 (C-1), 129.3, 128.6, 128.2, 127.9 (C-1″, C-2″, C-3″, C-4″, C-5″, C-6″), 127.5 (C-α), 119.9 (C-3′, C-5′), 115.3.4 (C-3, C-4, C-5), 70.1 (C-7″), 21.7 (C-7). HRMS (ESI): calcd. for $C_{15}H_{12}Br_2O_2S$ $[M + H]^+$ 328.1463, found 328.1443.

3.4. *In Vitro* Acetylcholinesterase Inhibitory Activities. Initially, dibasic sodium phosphate (Na_2HPO_4) (6.00 g) and monobasic sodium phosphate (NaH_2PO_4) (7.00 g) were dissolved in deionized water (500 mL) to form dibasic and monobasic solutions, respectively. Then, 0.1 M sodium phosphate buffers at pH 7.0 and 8.0 were prepared. For a buffer pH of 8.0, dibasic Na_2HPO_4 (93.2 mL) was mixed with monobasic NaH_2PO_4 (6.8 mL), while for a buffer pH of 7.0, dibasic Na_2HPO_4 (57.7 mL) was mixed with monobasic NaH_2PO_4 (42.3 mL). The pH of the two buffer solutions was adjusted to the desired pH by adding dibasic or monobasic solutions.[60]

The Ellman method was used to study the acetylcholinesterase (AChE) inhibitory activities of the synthesized compounds.[61] The reagents were freshly prepared before AChE inhibitory activity. First, 0.01 M DTNB was prepared by adding 5,5-dithio-bis(2-nitrobenzoic acid) (DTNB) (0.396 g) to sodium phosphate buffer (pH 7.0; 100 mL) and $NaHCO_3$ (0.0015 g). All the procedures were performed in the dark because DTNB is sensitive to light. Then, 0.075 M ATCI was prepared by dissolving ATCI (0.1024 g) in deionized water (5 mL). Next, 0.28 U/mL of AChE was prepared by adding 0.28 μL of AChE stock solution to sodium phosphate buffer (pH 8.0; 100 mL) and keeping it in an ice box. Samples (1 mg/mL) were prepared by dissolving them separately in 1 mL of methanol with 1 mg of the target compounds. In this study, galantamine hydrobromide was used as the positive control, so 1 mg of galantamine hydrobromide was dissolved in 1 mL of methanol.

A new microplate was labeled with samples, a positive control and blanks. There were three replicates for each sample, a positive control and blanks. First, 20 μL of sample, positive control or blank sample was injected into the microplate by using a suitable micropipette. Then, the microplate was wrapped with aluminum foil to avoid light contact, and 10 μL of DTNB was added to each sample, positive control and blank sample in the dark, followed by 15 μL of AChE enzyme and 140 μL of sodium phosphate buffer (pH 8.0). The solutions were incubated at 37°C for 15 minutes, after which 10 μL of ATCI was added to the samples, positive controls and blanks. After that, the microplate was incubated again for another 15 minutes before it was measured by a microplate reader at 412 nm. The plate was then read with an Epoch microplate reader at 412 nm. The activity was screened, and samples that gave 70% or more enzymatic inhibition were identified. The percentage of acetylcholinesterase inhibition was calculated using the formula below:

$$(\%)\text{Percentage inhibition} = 1 - \left[\left(\frac{\text{sample} - \text{blank}}{\text{sample}}\right) \times 100\right]$$

3.5. Computational Studies. *3.5.1. Molecular Docking.* Prior to being saved in *PDBQT* format using AutoDock Tools (v1.5.6rc3), the 3D structures of the synthesized derivatives (**12a-c**) were geometrically optimized utilizing the wB97XD/6-311++G(d,p) level of theory.[62] The process entails the following steps: Identifying the root of the torsion tree, selecting it, and recording the result as a pdpqt file for mapping purposes prior to performing a molecular docking simulation.

https://doi.org/10.1021/acsomega.4c03679
ACS Omega 2024, 9, 32901−32919

The crystallographic structure of AChE (PDB ID: 4EY7) was obtained from the protein database website (http://www.rcsb.org/pdb/). The protein structure was subjected to heteroatom removal, and molecular mechanics energy minimization was performed using Swiss-PdbViewer.[63] In the PDBQT format, the protein structure was prepared for molecular docking analysis.[64] Ultimately, a molecular docking simulation was conducted using the methodology described in prior studies.[10,31,65,66] Visualization and analysis were performed with Discovery Studio Visualizer software (Windows v21.1.0.20298) to create two-dimensional and three-dimensional figures illustrating ligand−receptor complex structures that depict such interactions.[67]

3.5.2. Molecular Dynamics Simulation (MDS). All-atom MD simulations were conducted on the compounds (**12a** and **12c**) with the highest consensus docking scores to examine the relative stabilities of the protein−ligand interactions and to screen compounds for additional binding energy calculations. Utilizing the GROMACS V2022.4 package[35,68,69] and the CHARMM36[70] force field, every simulation was conducted. The latest CHARMM/CGenFF force field was used to produce the parameters and topological files for the chosen compounds *via* CHARMM-GUI.[71] Utilizing a TIP3P explicit solvation model, the protein−ligand complex was submerged in the center of a box of solvated water molecules. 0.15 M ions (145 Na^+ and 135 Cl^-); to simulate the physiological salt concentrations found in the body, these ions were added to achieve charge neutralization and electrostatic screening, elongating up to 20 Å from the protein. With regard to the x, y, and z directions of the rectangular cubic system, the periodic boundary conditions and CHARMM were set with the following dimensions: 117.0, 117.0, and 117.0 Å, respectively.

In the MD protocols, equilibration, production, and minimization are all included. There were no atoms subjected to restraint during the 100 ns MD production simulations. For all MD simulations, the isothermal−isobaric (NPT) ensemble and a 2 fs time integration phase were utilized. The pressure was consistently maintained at 1 atm throughout the 100 ns of MD production utilizing the Nose'−Hoover Langevin piston barostat.[72] The Langevin thermostat was employed to regulate the temperature at 300.0 K.[73] We assumed that the force-field parameters excluded a scaling of 1.2 Å for the purpose of minimizing and equilibrating the complexes in the water box. Explicit illustrations were provided for all atoms, including hydrogen. After 5000 steps at a constant temperature (300 K), the preliminary energy of the complexes was reduced; subsequently, 144,000 additional steps were simulated, and Langevin dynamics were used to control the kinetic energy, temperature, and/or pressure of the system. Finally, 100 ns were required to equilibrate the solvated protein−ligand complex system with 500,000 steps and 50,000,000 runs. Every 25 ps, the structural coordinates were kept along the trajectories. Tools implemented in GROMACS and VMD were utilized to analyze the residues of the entire system, utilizing the trajectories recovered from the production step.[74] A distance cutoff of 20.0 Å was applied to short-range nonbonded interactions with a pair list distance of 1.2 Å, and Lennard Jones interactions were smoothly truncated at 8.0 Å. Long-range electrostatic interactions were treated using the particle−mesh Ewald (PME) method,[75] where a grid spacing of 1.0 Å was used for all simulation cells. For consistency, we applied the same protocol for all MD simulations.

3.5.3. DFT Computational Details. A molecular modeling calculation of three potential target derivatives of AChE inhibitors was performed during this investigation utilizing software packages, specifically the *Gaussian 09 W* package.[76] Density functional theory (DFT) with the long-range correction functional wB97XD (*DFT*/wB97XD), which incorporates empirical dispersion with the basis set 6-311++G (d, p),[77,78] was employed to geometrically optimize the molecular structures of the compounds under study. No symmetry constraints were enforced throughout the geometry optimization process.[79,80] As a result of the improved performance, consistency, accuracy, and flexibility of Grimme's D2 dispersion model, which incorporates empirical dispersion,[77,81] long-range correction functional wB97XD with a large basis set was selected. By using the same level of theory to compute the vibrational frequencies for each compound, it was found that the molecular structure of the target compounds aligns with the exact minimums of the potential energy surface. DFT/wB97XD was utilized to determine the reactivity descriptors and molecular stability with the purpose of identifying the reactive site of the molecules. The descriptor of the local reactivity was determined by calculating the dual descriptor and the Fukui function.[45−47,49−52] In addition, utilizing the Multiwfn v3.7 software program, the quantum chemical descriptors from conceptual density functional theory (CDFT) were computed.[55] The visual molecular dynamics package (VMD 1.9) was utilized to determine the electrostatic potential (ESP) of the molecules from the data produced by the Multiwfn program.[55,74] NBO 3.1, which was supplied in the Gaussian 09 W software program, was used for the natural bond orbital (NBO) analysis. To visualize the optimized structure and molecular orbitals, the ChemCraft (v1.6) and GaussView (v6.1) packages were utilized.[82,83] The SAR properties of the synthesized compounds were assessed utilizing the QSAR features integrated in the HyperChem program (v8.0.7).[84]

3.5.4. Binding Energy Calculations. Molecular mechanics energy techniques (MM/GBSA and MM/PBSA) are widely used to determine the free binding energies of small molecules to biological macromolecules.[31] The GBSA integrates the generalized Born and surface area continuum solvation models. On the other hand, the free energy of binding is computed using ensembles of the initial and final states in the one-average molecular mechanics Poisson−Boltzmann surface area (MM-PBSA) method, which is path-independent; consequently, MM-PBSA displays a greater level of efficacy than MMGBSA. To revalidate the inhibitory affinity of both ligands (60 and 64) for the AChE protein predicted by docking simulation experiments via molecular dynamics (MD) simulations via GROMACS, the binding free energy of the simulated complex was calculated. The binding free energies were computed by utilizing snapshots obtained from the system trajectories over a duration of 100 ns, after which the complex (*RL*) was formed when the ligand (*L*) bound to the protein receptor (*R*) using the gmx_MMPBSA tool, which is based on the AMBER tools MMPBSA.py and GROMACS files. We are solely concerned with conducting computations for relative binding energies. The Gibbs relative binding energy can be calculated as follows:[85]

$$\Delta G_{bind} = \Delta G_{RL} - \Delta G_R - \Delta G_L$$

https://doi.org/10.1021/acsomega.4c03679
ACS Omega 2024, 9, 32901−32919

4. CONCLUSIONS

4-Benzyloxychalcone derivatives **12a-c** were successfully synthesized *via* the Claisen Schmidt condensation reaction between appropriate aldehydes and ketones in the presence of NaOH as the basic catalyst. The titled compound molecular structures were confirmed using ATR-FTIR, NMR and HRMS analyses. Our study of anti-acetylcholinesterase activity revealed that the synthesized compounds were more potent than that of the standard drug galantamine. Furthermore, the molecular docking analysis demonstrated that the synthesized compounds engage in molecular interactions through hydrogen bonding, π-π T-shaped interactions and π-π stacking. These findings are consistent with the conclusion that **12a** and **12c** are promising candidates for AChE inhibitors, as determined by thorough examination of the patterns of binding sites and binding energies. Compound **12a** had the highest value according to the drug likeness and QSAR descriptors, whereas compound **12c** had the lowest values across all descriptors for the remaining derivatives. All the target compounds have weak oral bioavailability properties and require a drug delivery carrier to enhance oral properties. Furthermore, the log *P* values of compounds **12c** < **12b**< **12a** are outside the range of optimal values ($0 < Log\ P < 5$). The RMSD was utilized to measure the stability of the systems throughout the 100 ns simulations. These findings indicated that the conformation of the **12c** complex became more stable than that of the **12a** complex. The **12c**-AChE protein complex exhibited lower system inhibition than the other systems, as indicated by the calculated average RMSF values of 1.15 and 1.05 Å for the **12a**-AChE and **12c**-AChE complexes, respectively, for the protein systems. These findings are positively correlated with the stability of the complex.

The computation of binding free energy (MM/GBSA and MM/PBSA) was performed on the simulated complexes, and the calculated values for the **12c** complex and **12a** complex corresponded to mmgbsa and mmpbsa. Accordingly, the stability of the **12c**-4EY7 complex is suggested to be superior to that of the other complex. In light of the findings of the present study as a whole, **12a** could be a potential AChE candidate due to its ability to be used as a comparable or even superior descriptor to galantamine. Finally, a comprehensive understanding of the electronic structure properties, their correlation with drug-like properties, and the structure-activity relationships of the designed compounds were achieved through the utilization of a high number of computational techniques, such as DFT/wB97XD methods, with the basis set wave function 6-311++G(d,p).

■ ASSOCIATED CONTENT

Supporting Information

The Supporting Information is available free of charge at https://pubs.acs.org/doi/10.1021/acsomega.4c03679.

Additional figures illustrating the characterization of all synthesized compounds by IR,[1] H NMR, ^{13}C NMR, and mass spectra and computational studies (PDF)

■ AUTHOR INFORMATION

Corresponding Author

Joazaizulfazli Jamalis − *Department of Chemistry, Faculty of Science, Universiti Teknologi Malaysia, 81310 Johor Bahru, Johor, Malaysia;* orcid.org/0000-0002-1756-7244; Email: joazaizulfazli@utm.my

Authors

Helmi Mohammed Al-Maqtari − *Department of Chemistry, Faculty of Science, Universiti Teknologi Malaysia, 81310 Johor Bahru, Johor, Malaysia; Department of Chemistry, College of Education, Hodeidah University, Hodeidah, Yemen*

Aso Hameed Hasan − *Department of Chemistry, Faculty of Science, Universiti Teknologi Malaysia, 81310 Johor Bahru, Johor, Malaysia; Department of Chemistry, College of Science, University of Garmian, Kalar 46021 Kurdistan Region, Iraq*

Mustapha Suleiman − *Department of Chemistry, Faculty of Science, Universiti Teknologi Malaysia, 81310 Johor Bahru, Johor, Malaysia; Department of Chemistry, Sokoto state university, Sokoto 852101, Sokoto, Nigeria*

Muhammad Asraf Ahmad Zahidi − *Department of Chemistry, Faculty of Science, Universiti Teknologi Malaysia, 81310 Johor Bahru, Johor, Malaysia*

Mahmoud A. Noamaan − *Mathematics Department, Faculty of Science, Cairo University, Giza 12613, Egypt*

Pavel Alexyuk − *Research and Production Center for Microbiology and Virology, Almaty 050010, Kazakhstan*

Madina Alexyuk − *Research and Production Center for Microbiology and Virology, Almaty 050010, Kazakhstan*

Andrey Bogoyavlenskiy − *Research and Production Center for Microbiology and Virology, Almaty 050010, Kazakhstan;* orcid.org/0000-0001-9579-2298

Complete contact information is available at: https://pubs.acs.org/10.1021/acsomega.4c03679

Author Contributions

Aso Hameed Hasan, Mahmoud A. Noamaan, Muhammad Asraf Ahmad Zahidi, Pavel Alexyuk, Joazaizulfazli Jamalis, and Andrey Bogoyavlenskiy had full access to all of the data in the study and take responsibility for the integrity of the data and the accuracy of the data analysis. Concept and design: Andrey Bogoyavlenskiy, Madina Alexyuk, Helmi Mohammed Al-Maqtari, and Mustapha Suleiman. Acquisition, analysis, or interpretation of data: Joazaizulfazli Jamalis and Madina Alexyuk. Drafting of the manuscript: Helmi Mohammed Al-Maqtari, Aso Hameed Hasan and Mustapha Suleiman. Critical revision of the manuscript for important intellectual content: All authors. Statistical analysis: All authors.

Funding

This work was supported by the Ministry of Science and Higher Education of the Republic of Kazakhstan AP19678025 "Comparative study of the immunomodulatory effect of organic acids, triterpenes and flavonoids in the treatment of viral diseases"

Notes

The authors declare no competing financial interest.

■ ACKNOWLEDGMENTS

The authors wish to thank the Ministry of Science and Higher Education of the Republic of Kazakhstan AP19678025 "Comparative study of the immunomodulatory effect of organic acids, triterpenes and flavonoids in the treatment of viral diseases"

■ REFERENCES

(1) Siddiqa, A.; Tajammal, A.; Irfan, A.; Azam, M.; Munawar, M. A.; Hardy, R. S.; Basra, M. A. R. Synthesis, molecular docking, bio-evaluation and quantitative structure activity relationship of new

chalcone derivatives as antioxidants. *Journal of Molecular Structure* **2023**, *1277*, No. 134814.
(2) Abdalla Ali, A.; Mhamad, S. A.; Hasan, A. H.; Ahmad, I.; Abdullah, S. A.; Jamil, S.; Patel, H.; Murugesan, S.; Jamalis, J. Synthesis, biological evaluation and molecular modeling studies of modulated benzyloxychalcones as potential acetylcholinesterase inhibitors. *Journal of Biomolecular Structure and Dynamics* **2024**, *42*, 3604−3615.
(3) Ávila, H. P.; Smânia, E. d. F. A.; Delle Monache, F.; Smânia, A. Structureactivity relationship of antibacterial chalcones. *Bioorganic & medicinal chemistry* **2008**, *16* (22), 9790−9794.
(4) Rayees Ahmad, M.; Girija Sastry, V.; Bano, N.; Anwar, S. Synthesis of novel chalcone derivatives by conventional and microwave irradiation methods and their pharmacological activities. *Arabian Journal of Chemistry* **2016**, *9*, S931−S935.
(5) Mezgebe, K.; Melaku, Y.; Mulugeta, E. Synthesis and Pharmacological Activities of Chalcone and Its Derivatives Bearing N-Heterocyclic Scaffolds: A Review. *ACS Omega* **2023**, *8* (22), 19194−19211.
(6) Cazarolli, L. H.; Kappel, V. D.; Zanatta, A. P.; Suzuki, D. O. H.; Yunes, R. A.; Nunes, R. J.; Pizzolatti, M. G.; Silva, F. R. M. B. Natural and Synthetic Chalcones: Tools for the Study of Targets of Action—Insulin Secretagogue or Insulin Mimetic? *Studies in Natural Products Chemistry* **2013**, *39*, 47−89.
(7) Salih, R. H. H.; Hasan, A. H.; Hussen, N. H.; Hawaiz, F. E.; Hadda, T. B.; Jamalis, J.; Almalki, F. A.; Adeyinka, A. S.; Coetzee, L.-C. C.; Oyebamiji, A. K. Thiazole-pyrazoline hybrids as potential antimicrobial agent: Synthesis, biological evaluation, molecular docking, DFT studies and POM analysis. *Journal of Molecular Structure* **2023**, *1282*, No. 135191.
(8) Mathew, B.; Suresh, J.; Anbazghagan, S.; Paulraj, J.; Krishnan, G. K. Heteroaryl chalcones: Mini review about their therapeutic voyage. *Biomedicine & Preventive Nutrition* **2014**, *4* (3), 451−458.
(9) Suyambulingam, A.; Nair, S.; Chellapandian, K. Synthesis, spectral characterization of novel chalcones based oxazines derivatives and screening of their antimicrobial and antioxidant activity. *Journal of Molecular Structure* **2022**, *1268*, No. 133708.
(10) Hasan, A. H.; Murugesan, S.; Amran, S. I.; Chander, S.; Alanazi, M. M.; Hadda, T. B.; Shakya, S.; Pratama, M. R. F.; Das, B.; Biswas, S.; Jamalis, J. Novel thiophene Chalcones-Coumarin as acetylcholinesterase inhibitors: Design, synthesis, biological evaluation, molecular docking, ADMET prediction and molecular dynamics simulation. *Bioorganic Chemistry* **2022**, *119*, No. 105572.
(11) Rozmer, Z.; Perjési, P. Naturally occurring chalcones and their biological activities. *Phytochemistry Reviews* **2016**, *15* (1), 87−120.
(12) Jiwrajka, M.; Phillips, A.; Butler, M.; Rossi, M.; Pocock, J. M. The Plant-Derived Chalcone 2,2′,5′-Trihydroxychalcone Provides Neuroprotection against Toll-Like Receptor 4 Triggered Inflammation in Microglia. *Oxidative Medicine and Cellular Longevity* **2016**, *2016*, No. 6301712.
(13) Hasan, A. H.; Amran, S. I.; Hussain, F. H. S.; Jaff, B. A.; Jamalis, J. Molecular Docking and Recent Advances in the Design and Development of Cholinesterase Inhibitor Scaffolds: Coumarin Hybrids. *ChemistrySelect* **2019**, *4* (48), 14140−14156.
(14) Campora, M.; Francesconi, V.; Schenone, S.; Tasso, B.; Tonelli, M. Journey on Naphthoquinone and Anthraquinone Derivatives: New Insights in Alzheimer's Disease. *Pharmaceuticals* **2021**, *14* (1), 33.
(15) Lane, R. M.; Potkin, S. G.; Enz, A. Targeting acetylcholinesterase and butyrylcholinesterase in dementia. *International Journal of Neuropsychopharmacology* **2006**, *9* (1), 101−124.
(16) Marucci, G.; Buccioni, M.; Ben, D. D.; Lambertucci, C.; Volpini, R.; Amenta, F. Efficacy of acetylcholinesterase inhibitors in Alzheimer's disease. *Neuropharmacology* **2021**, *190*, No. 108352.
(17) Sharma, K. Cholinesterase inhibitors as Alzheimer's therapeutics (Review). *Mol Med Rep* **2019**, *20* (2), 1479−1487.
(18) Liu, S.; Chen, L.; Li, J.; Sun, Y.; Xu, Y.; Li, Z.; Zhu, Z.; Li, X. Asiaticoside Mitigates Alzheimer's Disease Pathology by Attenuating Inflammation and Enhancing Synaptic Function. *International Journal of Molecular Sciences* **2023**, *24* (15), 11976.
(19) Dzoyem, J. P.; Nkuete, A. H. L.; Ngameni, B.; Eloff, J. N. Anti-inflammatory and anticholinesterase activity of six flavonoids isolated from Polygonum and Dorstenia species. *Archives of Pharmacal Research* **2017**, *40* (10), 1129−1134.
(20) Ghribia, L.; Ghouilaa, H.; Omrib, A.; Besbesb, M.; Janneta, H. B. Antioxidant and anti−acetylcholinesterase activities of extracts and secondary metabolites from Acacia cyanophylla. *Asian Pacific Journal of Tropical Biomedicine* **2014**, *4*, S417−S423.
(21) Sribuhom, T.; Saraphon, C.; Decharchoochart, P.; Boonyarat, C.; Yenjai, C. Acetylcholinesterase inhibition and cytotoxicity of flavonoids and chalcones from Derris indica. *ScienceAsia* **2016**, *42* (4), 247−251.
(22) Hasan, A. H.; Shakya, S.; Hussain, F. H. S.; Murugesan, S.; Chander, S.; Pratama, M. R. F.; Jamil, S.; Das, B.; Biswas, S.; Jamalis, J. Design, synthesis, anti-acetylcholinesterase evaluation and molecular modelling studies of novel coumarin-chalcone hybrids. *Journal of Biomolecular Structure and Dynamics* **2023**, *41* (21), 11450−11462.
(23) Abdel-Rahman, A. A.-H.; Abdel-Megied, A. E.-S.; Hawata, M. A. M.; Kasem, E. R.; Shabaan, M. T. Synthesis and antimicrobial evaluation of some chalcones and their derived pyrazoles, pyrazolines, isoxazolines, and 5, 6-dihydropyrimidine-2-(1H)-thiones. *Monatshefte für Chemie-Chemical Monthly* **2007**, *138* (9), 889−897.
(24) Chen, Y.-H.; Wang, W.-H.; Wang, Y.-H.; Lin, Z.-Y.; Wen, C.-C.; Chern, C.-Y. Evaluation of the anti-inflammatory effect of chalcone and chalcone analogues in a zebrafish model. *Molecules* **2013**, *18* (2), 2052−2060.
(25) Koohmareh, G. A.; Mirkhani, V.; Fallah, H. R.; Sajadi, S. M. S. Synthesis, characterization, and optical properties of new pyridine-and thiophene-based copolymer bearing bulky naphthyl group. *Polymer Bulletin* **2015**, *72* (11), 2979−2990.
(26) Khan, S. A.; Asiri, A. M. Green synthesis, characterization and biological evaluation of novel chalcones as anti bacterial agents. *Arabian Journal of Chemistry* **2017**, *10*, S2890−S2895.
(27) Freeman, J. V.; Dewey, F. E.; Hadley, D. M.; Myers, J.; Froelicher, V. F. Autonomic Nervous System Interaction With the Cardiovascular System During Exercise. *Progress in Cardiovascular Diseases* **2006**, *48* (5), 342−362.
(28) Lilienfeld, S. Galantamine — a Novel Cholinergic Drug with a Unique Dual Mode of Action for the Treatment of Patients with Alzheimer's Disease. *CNS Drug Reviews* **2002**, *8* (2), 159−176.
(29) Mirzaei, S.; Eisvand, F.; Hadizadeh, F.; Mosaffa, F.; Ghasemi, A.; Ghodsi, R. Design, synthesis and biological evaluation of novel 5,6,7-trimethoxy-N-aryl-2-styrylquinolin-4-amines as potential anti-cancer agents and tubulin polymerization inhibitors. *Bioorganic Chemistry* **2020**, *98*, No. 103711.
(30) Miller, J. N. Coumarin-6-sulphonyl chloride: a novel label in fluorimetry and phosphorimetry Part 1. Synthesis and Luminescence Properties. *Analytica Chimica Acta* **1989**, *227*, 145−153.
(31) Hasan, A. H.; Abdulrahman, F. A.; Obaidullah, A. J.; Alotaibi, H. F.; Alanazi, M. M.; Noamaan, M. A.; Murugesan, S.; Amran, S. I.; Bhat, A. R.; Jamalis, J. Discovery of Novel Coumarin-Schiff Base Hybrids as Potential Acetylcholinesterase Inhibitors: Design, Synthesis, Enzyme Inhibition, and Computational Studies. *Pharmaceuticals* **2023**, *16* (7), 971.
(32) Kumari, R.; Kumar, R.; Lynn, A. g_mmpbsa—A GROMACS Tool for High-Throughput MM-PBSA Calculations. *Journal of Chemical Information and Modeling* **2014**, *54* (7), 1951−1962.
(33) Pronk, S.; Páll, S.; Schulz, R.; Larsson, P.; Bjelkmar, P.; Apostolov, R.; Shirts, M. R.; Smith, J. C.; Kasson, P. M.; van der Spoel, D.; Hess, B.; Lindahl, E. GROMACS 4.5: a high-throughput and highly parallel open source molecular simulation toolkit. *Bioinformatics* **2013**, *29* (7), 845−854.
(34) Valdés-Tresanco, M. S.; Valdés-Tresanco, M. E.; Valiente, P. A.; Moreno, E. gmx_MMPBSA: A New Tool to Perform End-State Free Energy Calculations with GROMACS. *Journal of Chemical Theory and Computation* **2021**, *17* (10), 6281−6291.
(35) Berendsen, H. J. C.; van der Spoel, D.; van Drunen, R. GROMACS: A message-passing parallel molecular dynamics

https://doi.org/10.1021/acsomega.4c03679
ACS Omega 2024, 9, 32901−32919

implementation. *Computer Physics Communications* **1995**, *91* (1), 43−56.
(36) Andrasi, M.; Buglyo, P.; Zekany, L.; Gaspar, A. A comparative study of capillary zone electrophoresis and pH-potentiometry for determination of dissociation constants. *Journal of Pharmaceutical and Biomedical Analysis* **2007**, *44* (5), 1040−1047.
(37) Khaled, D. M.; Elshakre, M. E.; Noamaan, M. A.; Butt, H.; Abdel Fattah, M. M.; Gaber, D. A. A Computational QSAR, Molecular Docking and In Vitro Cytotoxicity Study of Novel Thiouracil-Based Drugs with Anticancer Activity against Human-DNA Topoisomerase II. *International Journal of Molecular Sciences* **2022**, *23* (19), 11799.
(38) Elshakre, M. E.; Noamaan, M. A.; Moustafa, H.; Butt, H. Density Functional Theory, Chemical Reactivity, Pharmacological Potential and Molecular Docking of Dihydrothiouracil-Indenopyridopyrimidines with Human-DNA Topoisomerase II. *International Journal of Molecular Sciences* **2020**, *21* (4), 1253.
(39) Belaidi, S.; Belaidi, H.; Bouzidi, D. Computational Methods Applied in Physical-Chemistry Property Relationships of Thiophene Derivatives. *Journal of Computational and Theoretical Nanoscience* **2015**, *12* (8), 1737−1745.
(40) Arai, H.; Higashigaki, Y.; Gotoh, M.; Seiki Yano, S. Y. Structural Properties of Some Cyanoethenes with Optical Nonlinearity. *Japanese Journal of Applied Physics* **1994**, *33* (10R), 5755.
(41) Khan, S. A.; Rizwan, K.; Shahid, S.; Noamaan, M. A.; Rasheed, T.; Amjad, H. Synthesis, DFT, computational exploration of chemical reactivity, molecular docking studies of novel formazan metal complexes and their biological applications. *Applied Organometallic Chemistry* **2020**, *34* (3), No. e5444.
(42) Pearson, R. G. Absolute electronegativity and hardness correlated with molecular orbital theory. *Proceedings of the National Academy of Sciences* **1986**, *83* (22), 8440−8441.
(43) Parr, R.; Yang, W. *Density-functional theory of atoms and molecules*; Oxford university press: New York, NY, 1989.
(44) Mendoza-Huizar, L. H.; Rios-Reyes, C. H. Chemical reactivity of atrazine employing the Fukui function. *Journal of the Mexican Chemical Society* **2011**, *55* (3), 142−147.
(45) Chattaraj, P. K.; Roy, D. R. Update 1 of: Electrophilicity Index. *Chemical Reviews* **2007**, *107* (9), PR46−PR74.
(46) Geerlings, P.; De Proft, F.; Langenaeker, W. Conceptual Density Functional Theory. *Chemical Reviews* **2003**, *103* (5), 1793−1874.
(47) Parr, R. G.; Yang, W. Density functional approach to the frontier-electron theory of chemical reactivity. *Journal of the American Chemical Society* **1984**, *106* (14), 4049−4050.
(48) Liu, S.-B. Conceptual Density Functional Theory and Some Recent Developments. *Acta Physico-Chimica Sinica* **2009**, *25* (3), 590−600.
(49) Parr, R. G.; Pearson, R. G. Absolute hardness: companion parameter to absolute electronegativity. *Journal of the American Chemical Society* **1983**, *105* (26), 7512−7516.
(50) Chattaraj, P. K.; Giri, S. Stability, Reactivity, and Aromaticity of Compounds of a Multivalent Superatom. *The Journal of Physical Chemistry A* **2007**, *111* (43), 11116−11121.
(51) Contreras, R. R.; Fuentealba, P.; Galván, M.; Pérez, P. A direct evaluation of regional Fukui functions in molecules. *Chemical Physics Letters* **1999**, *304* (5), 405−413.
(52) Morell, C.; Grand, A.; Toro-Labbé, A. New Dual Descriptor for Chemical Reactivity. *The Journal of Physical Chemistry A* **2005**, *109* (1), 205−212.
(53) Parthasarathi, R.; Padmanabhan, J.; Elango, M.; Subramanian, V.; Chattaraj, P. K. Intermolecular reactivity through the generalized philicity concept. *Chemical Physics Letters* **2004**, *394* (4), 225−230.
(54) Lee, C.; Yang, W.; Parr, R. G. Local softness and chemical reactivity in the molecules CO, SCN− and H2CO. *Journal of Molecular Structure: THEOCHEM* **1988**, *163*, 305−313.
(55) Lu, T.; Chen, F. Multiwfn: A multifunctional wavefunction analyzer. *Journal of Computational Chemistry* **2012**, *33* (5), 580−592.
(56) Naray-Szabo, G.; Ferenczy, G. G. Molecular Electrostatics. *Chemical Reviews* **1995**, *95* (4), 829−847.
(57) Murray, J. S.; Politzer, P. The electrostatic potential: an overview. *WIREs Computational Molecular Science* **2011**, *1* (2), 153−163.
(58) Anbukarasi, K.; Xavier, S.; Hasan, H. A.; Er, L. Y.; Jamalis, J.; Sebastian, S.; Periandy, S. DFT and Molecular Docking Analysis of Newly Synthesized Compound (2E)-3-[3-(Benzyloxy) Phenyl]-1-(4′-Chlorophe-Nyl)-2-Propen-1-One [Bpclpo]. *Current Physical Chemistry* **2023**, *13*, 37−74.
(59) Luque, F. J.; López, J. M.; Orozco, M. Perspective on "Electrostatic interactions of a solute with a continuum. A direct utilization of ab initio molecular potentials for the prevision of solvent effects. *Theoretical Chemistry Accounts* **2000**, *103* (3), 343−345.
(60) Hasan, H. A.; Yusof, S. M. F.; Kamarudin, A. N.; Murugesan, S.; Shakya, S.; Jamalis, J. Synthesis, Anti-acetylcholinesterase Evaluation, Molecular Docking and Molecular Dynamics Simulation of Novel Psoralen Derivatives. *Current Organic Synthesis* **2024**, *21*, 61−77.
(61) Ellman, G. L.; Courtney, K. D.; Andres, V.; Featherstone, R. M. A new and rapid colorimetric determination of acetylcholinesterase activity. *Biochemical Pharmacology* **1961**, *7* (2), 88−95.
(62) Morris, G. M.; Goodsell, D. S.; Halliday, R. S.; Huey, R.; Hart, W. E.; Belew, R. K.; Olson, A. J. Automated docking using a Lamarckian genetic algorithm and an empirical binding free energy function. *Journal of Computational Chemistry* **1998**, *19* (14), 1639−1662.
(63) Guex, N.; Peitsch, M. C. SWISS-MODEL and the Swiss-PdbViewer: an environment for comparative protein modeling. *Electrophoresis* **1997**, *18* (15), 2714−23.
(64) Hussen, H. N.; Hamid, J. S.; Sabir, N. M.; Hasan, H. A.; Mohammed, J. S.; Shali, A. K. A. Novel Penicillin Derivatives Against Selected Multiple-Drug Resistant Bacterial Strains: Design, Synthesis, Structural Analysis, in silico and in Vitro Studies. *Current Organic Synthesis* **2024**, *21*, 684−703.
(65) Hasan, A. H.; Hussen, N. H.; Shakya, S.; Jamalis, J.; Pratama, M. R. F.; Chander, S.; Kharkwal, H.; Murugesan, S. In silico discovery of multi-targeting inhibitors for the COVID-19 treatment by molecular docking, molecular dynamics simulation studies, and ADMET predictions. *Structural Chemistry* **2022**, *33*, 1645−1665.
(66) Hamaamin Hussen, N. H.; Hameed Hasan, A. H.; Jamalis, J.; Shakya, S.; Chander, S.; Kharkwal, H.; Murugesan, S.; Ajit Bastikar, V.; Pyarelal Gupta, P. Potential inhibitory activity of phytoconstituents against black fungus: In silico ADMET, molecular docking and MD simulation studies. *Computational Toxicology* **2022**, *24*, No. 100247.
(67) Dassault systèmes. *BIOVIA discovery studio visualizer*, v. *172*, Dassault Systèmes: San Diego, 2016.
(68) Abraham, M. J.; Murtola, T.; Schulz, R.; Páll, S.; Smith, J. C.; Hess, B.; Lindahl, E. GROMACS: High performance molecular simulations through multi-level parallelism from laptops to supercomputers. *SoftwareX* **2015**, *1-2*, 19−25.
(69) Páll, S.; Abraham, M. J.; Kutzner, C.; Hess, B.; Lindahl, E. Tackling Exascale Software Challenges in Molecular Dynamics Simulations with GROMACS. *Solving Software Challenges for Exascale* **2015**, *8759*, 3−27.
(70) Best, R. B.; Zhu, X.; Shim, J.; Lopes, P. E. M.; Mittal, J.; Feig, M.; MacKerell, A. D., Jr. Optimization of the Additive CHARMM All-Atom Protein Force Field Targeting Improved Sampling of the Backbone ϕ, ψ and Side-Chain χ1 and χ2 Dihedral Angles. *Journal of Chemical Theory and Computation* **2012**, *8* (9), 3257−3273.
(71) Lee, J.; Cheng, X.; Swails, J. M.; Yeom, M. S.; Eastman, P. K.; Lemkul, J. A.; Wei, S.; Buckner, J.; Jeong, J. C.; Qi, Y.; Jo, S.; Pande, V. S.; Case, D. A.; Brooks, C. L., III; MacKerell, A. D., Jr.; Klauda, J. B.; Im, W. CHARMM-GUI Input Generator for NAMD, GROMACS, AMBER, OpenMM, and CHARMM/OpenMM Simulations Using the CHARMM36 Additive Force Field. *Journal of Chemical Theory and Computation* **2016**, *12* (1), 405−413.
(72) Nosé, S.; Klein, M. L. Constant pressure molecular dynamics for molecular systems. *Molecular Physics* **1983**, *50* (5), 1055−1076.

https://doi.org/10.1021/acsomega.4c03679
ACS Omega 2024, 9, 32901−32919

(73) Grest, G. S.; Kremer, K. Molecular dynamics simulation for polymers in the presence of a heat bath. *Physical Review A* **1986**, *33* (5), 3628−3631.
(74) Humphrey, W.; Dalke, A.; Schulten, K. VMD: Visual molecular dynamics. *Journal of Molecular Graphics* **1996**, *14* (1), 33−38.
(75) Essmann, U.; Perera, L.; Berkowitz, M. L.; Darden, T.; Lee, H.; Pedersen, L. G. A smooth particle mesh Ewald method. *The Journal of Chemical Physics* **1995**, *103* (19), 8577−8593.
(76) Frisch, M. J.; Trucks, G. W.; Schlegel, H. B.; Scuseria, G. E.; Robb, M. A.; Cheeseman, J. R.; Scalmani, G.; Barone, V.; Mennucci, B.; Petersson, G. A.; Nakatsuji, H.; Caricato, M.; Li, X.; Hratchian, H. P.; Izmaylov, A. F.; Bloino, J.; Zheng, G.; Sonnenberg, J. L.; Hada, M.; Ehara, M.; Toyota, K.; Fukuda, R.; Hasegawa, J.; Ishida, M.; Nakajima, T.; Honda, Y.; Kitao, O.; Nakai, H.; Vreven, T.; Montgomery, J. A., Jr.; Peralta, J. E.; Ogliaro, F.; Bearpark, M.; Heyd, J. J.; Brothers, E.; Kudin, K. N.; Staroverov, V. N.; Kobayashi, R.; Normand, J.; Raghavachari, K.; Rendell, A.; Burant, J. C.; Iyengar, S. S.; Tomasi, J.; Cossi, M.; Rega, N.; Millam, J. M.; Klene, M.; Knox, J. E.; Cross, J. B.; Bakken, V.; Adamo, C.; Jaramillo, J.; Gomperts, R.; Stratmann, R. E.; Yazyev, O.; Austin, A. J.; Cammi, R.; Pomelli, C.; Ochterski, J. W.; Martin, R. L.; Morokuma, K.; Zakrzewski, V. G.; Voth, G. A.; Salvador, P.; Dannenberg, J. J.; Dapprich, S.; Daniels, A. D.; Farkas, O.; Foresman, J. B.; Ortiz, J. V.; Cioslowski, J.; Fox, D. J. *Gaussian 09*, revision E.01; Gaussian, Inc.: Wallingford, CT, 2009.
(77) Chai, J.-D.; Head-Gordon, M. Long-range corrected hybrid density functionals with damped atom−atom dispersion corrections. *Physical Chemistry Chemical Physics* **2008**, *10* (44), 6615−6620.
(78) McLean, A. D.; Chandler, G. S. Contracted Gaussian basis sets for molecular calculations. I. Second row atoms, Z=11−18. *The Journal of Chemical Physics* **1980**, *72* (10), 5639−5648.
(79) Reed, A. E.; Weinhold, F. Natural bond orbital analysis of near-Hartree−Fock water dimer. *The Journal of Chemical Physics* **1983**, *78* (6), 4066−4073.
(80) Ulic, S. E.; Védova, C. O. D.; Hermann, A.; Mack, H.-G.; Oberhammer, H. Preparation and Properties of Trifluorothioacetic Acid- S-(trifluoromethyl)ester, CF 3C(O)SCF 3. *The Journal of Physical Chemistry A* **2008**, *112* (27), 6211−6216.
(81) Lin, Y.-S.; Li, G.-D.; Mao, S.-P.; Chai, J.-D. Long-Range Corrected Hybrid Density Functionals with Improved Dispersion Corrections. *Journal of Chemical Theory and Computation* **2013**, *9* (1), 263−272.
(82) *GaussView*, (Version 6.1), Dennington, R.; Keith, T. A.; Millam, J., Semichem Inc., Shawnee Mission, KS, 2016.
(83) *Chemcraft - graphical software for visualization of quantum chemistry computations*. https://www.chemcraftprog.com.
(84) Froimowitz, M. HyperChem: a software package for computational chemistry and molecular modeling. *Biotechniques* **1993**, *14* (6), 1010−1013.
(85) Wang, E.; Sun, H.; Wang, J.; Wang, Z.; Liu, H.; Zhang, J. Z. H.; Hou, T. End-Point Binding Free Energy Calculation with MM/PBSA and MM/GBSA: Strategies and Applications in Drug Design. *Chemical Reviews* **2019**, *119* (16), 9478−9508.

https://doi.org/10.1021/acsomega.4c03679
ACS Omega 2024, 9, 32901−32919